

COLLECTION, FOCUSING, AND METERING OF DNA IN MICROCHANNELS  
USING ADDRESSABLE ELECTRODE ARRAYS FOR PORTABLE LOW-POWER  
BIOANALYSIS

A Dissertation

by

FAISAL SHAIKH

Submitted to the Office of Graduate Studies of  
Texas A&M University  
in partial fulfillment of the requirements for the degree of

DOCTOR OF PHILOSOPHY

August 2008

Major Subject: Chemical Engineering

COLLECTION, FOCUSING, AND METERING OF DNA IN MICROCHANNELS  
USING ADDRESSABLE ELECTRODE ARRAYS FOR PORTABLE LOW-POWER  
BIOANALYSIS

A Dissertation

by

FAISAL SHAIKH

Submitted to the Office of Graduate Studies of  
Texas A&M University  
in partial fulfillment of the requirements for the degree of

DOCTOR OF PHILOSOPHY

Approved by:

Chair of Committee,	Victor M. Ugaz
Committee Members,	Gyula Vigh
	Yue Kuo
	Arul Jayaraman
Head of Department,	Michael Pishko

August 2008

Major Subject: Chemical Engineering



## ABSTRACT

Collection, Focusing, and Metering of DNA in Microchannels Using Addressable  
Electrode Arrays for Portable Low-Power Bioanalysis. (August 2008)

B.En., University of Mumbai, Institute of Chemical Technology, Mumbai, India.

Chair of Advisory Committee: Dr. Victor M. Ugaz

Although advances in microfluidic technology have enabled increasingly sophisticated biosensing and bioassay operations to be performed at the microscale, many of these applications employ such small amounts of charged biomolecules (DNA, proteins, peptides) that they must first be pre-concentrated to a detectable level. Efficient strategies for precisely handling minute quantities of biomolecules in microchannel geometries are critically needed, however it has proven challenging to achieve simultaneous concentration, focusing, and metering capabilities with current-generation sample injection technology. Using microfluidic chips incorporating arrays of individually addressable microfabricated electrodes, we demonstrate that DNA can be sequentially concentrated, focused into a narrow zone, metered, and injected into an analysis channel.

The technique used in this research transports charged biomolecules between active electrodes upon application of a small potential difference (1 V), and is capable of achieving orders of magnitude concentration increases within a small device footprint. The collected samples are highly focused, with sample zone size and shape defined

solely by electrode geometry. In addition to achieving the objectives of the research project, this setup was found to provide added functionality as a label-free biomolecule detection technique due to the formation of light scattering phases of charged biomolecules on top of the capture electrode.

## DEDICATION

I dedicate this dissertation to my parents who have supported my educational upbringing throughout my life.

## ACKNOWLEDGEMENTS

I would like to thank my committee chair, Dr. Ugaz, and my committee members, Prof. Vigh, Dr. Jayaraman, and Prof. Kuo, for their guidance and support throughout the course of this research. I would like to express my deep gratitude to Dr. Ugaz for his patience, frankness, overall guidance and dedication to this work. Prof. Vigh's suggestions on testing the label-free detection technique with specific chemical entities that he provided are aiding, in ongoing work, in getting a better understanding of the physical and mechanistic aspects of the label-free detection process. I had helpful and very insightful discussions with him, regarding the possibilities of the physical mechanisms involved in the process.

Thanks also go to my brother Faiz who helped with his coding skills to program a handheld interface for the lab-on-a-chip studied in this research. My stay in College Station was enjoyable, thanks to the numerous friendships I was lucky to have made here. Noor, Mert, Kamran, Hans, Omar, Ferdi, Roger, Serdar, Abdullah, Renat, Jian, Xiaojia, Sumit, Khalid, Mohsin, Harshal and Sanjay have been great colleagues and friends throughout my stay here. I thank the department faculty and staff, especially Prof. Mahmoud El-Halwagi and Towanna for making my time at Texas A&M University a great experience. I also want to extend my gratitude to the National Science Foundation, for providing the funding for this work.

## NOMENCLATURE

DNA	Deoxyribonucleic Acid
dsDNA	Double Stranded DNA
ssDNA	Single Stranded DNA
EDTA	Ethylene Diamine Tetracetic Acid
TBE	Tris-Borate EDTA
BME	Beta Mercapto Ethanol
PCB	Printed Circuit Board
DI	Deionized
UV	Ultraviolet
RIE	Reactive Ion Etcher
CCD	Charge Coupled Device
PC	Personal Computer
HMDS	Hexamethyldisilazane

## TABLE OF CONTENTS

	Page
ABSTRACT .....	iii
DEDICATION .....	v
ACKNOWLEDGEMENTS .....	vi
NOMENCLATURE .....	vii
TABLE OF CONTENTS.....	viii
LIST OF FIGURES.....	xi
LIST OF TABLES.....	xiv
I INTRODUCTION.....	1
II DNA CONCENTRATION AND FOCUSING IN MICROCHANNELS.....	4
2.1 Background.....	4
2.2 Literature.....	5
2.3 The Capture-Release Approach .....	9
2.4 Dual Focus and Metering.....	11
2.5 Characterization and Analysis.....	14
III DNA INJECTION INTO MICROCHANNELS .....	19
3.1 Background and Significance .....	19
3.2 Capture-Release Injection.....	19
3.3 Enhanced Electrophoresis Resolution on Microfabricated Chip .....	22
IV DEVICE DESIGN AND OPERATION .....	25
4.1 Device Components.....	25
4.2 Microchip Fabrication and Assembly .....	28
4.3 Preparation of DNA Samples.....	29
4.4 Microdevice Usage.....	33
4.5 Imaging and Detection.....	33
4.6 The Electrode Array .....	35

	Page
V FINITE ELEMENT ANALYSIS SIMULATION.....	37
5.1 Introduction.....	37
5.2 Model Development and Results .....	38
VI LABEL-FREE DETECTION OF CHARGED BIOMOLECULES.....	43
6.1 On-Chip Detection Strategies in Literature.....	43
6.2 Experimental Observations of Label-Free DNA Detection on the Capture Electrode.....	44
6.3 Fundamental Characterization of the Optical Phenomenon .....	46
6.3.1 Mesophase Formation .....	47
6.3.2 Experimentation and Results .....	47
6.3.3 Device Design.....	52
6.3.4 Calculation of Critical Concentrations of Mesophase Formation .....	54
6.3.5 Refractive Index Change.....	55
6.3.6 Directions for Further Characterization .....	57
6.4 Label-free Protein (Lysozyme) Detection .....	58
VII ADVANCED APPLICATIONS .....	61
7.1 Buffer Exchange.....	61
7.2 Possibilities for Application of Capture-Release .....	63
VIII PORTABLE INTERFACE FOR LAB-ON-A-CHIP .....	65
8.1 Field Programmable Gate Array (FPGA).....	65
8.2 Programming and Operation.....	68
IX CONCLUSIONS .....	73
REFERENCES.....	76
APPENDIX A PRINTED CIRCUIT BOARD FABRICATION PROCEDURE.....	81
APPENDIX B FABRICATION OF SILICON DEVICES.....	83
APPENDIX C MASK ALIGNER INSTRUCTIONS.....	87
APPENDIX D FABRICATION OF GLASS CHANNELS.....	90

	Page
APPENDIX E WIRE BONDING PROCEDURE .....	94
APPENDIX F WAFER DICING OF SILICON AND GLASS WAFERS .....	96
VITA.....	104



## LIST OF FIGURES

		Page
Figure 1	Simultaneous concentration and focusing of DNA using an array of individually addressable microelectrodes.....	10
Figure 2	Snapshot of the capture of DNA showing the dual focus applied by applying opposing electric field on both sides of the capture electrode leading to the highly focused DNA plug .....	12
Figure 3	The increase in concentration at each subsequent electrode in the array is indicated by increases in the detected normalized fluorescence intensity .....	13
Figure 4	Metering of DNA sample achieved by simultaneously applying the dual focus at a number of neighboring electrodes .....	14
Figure 5	The achievable concentration as indicated by normalized level of fluorescence intensity is robust and essentially independent of buffer composition, amount of BME, and electrode material.....	16
Figure 6	The influence of focusing and concentration of an injected sample on the ability to detect and resolve two distinct components by electrophoretic separation .....	21
Figure 7	Effect of the pre-concentration and focusing process on the separation resolution.....	24
Figure 8	Exploded view of the capture-release chip showing device components. ....	26
Figure 9	Assembled capture-release chip showing the electrode array.....	27
Figure 10	A 6 inch silicon wafer after lithography, gold deposition and dicing .....	30
Figure 11	A close up image of the capture-release device revealing the assembly of various components .....	31
Figure 12	A microscopic image of the device showing the access holes for sample inlet and the epoxy used to safeguard the wire bonds .....	32

	Page
Figure 13	Experimental set-up showing the optical microscope with the attached CCD camera and stage control interfaced to the computer. 34
Figure 14	The electrode array as seen under a microscope..... 36
Figure 15	Electrode capture process simulated for DNA initially at 12 $\mu\text{g/ml}$ in 1x TBE buffer under a 1 V applied potential..... 41
Figure 16	DNA visible under white light (100 bp DNA ladder in 1X TBE buffer) ..... 45
Figure 17	Schematic illustration of the label free DNA detection in free solution..... 45
Figure 18	The lab-chip on the left shows the addressable electrode array along the microchannel floor ..... 46
Figure 19	A schematic of the compaction of DNA occurring during the dual-focus..... 48
Figure 20	Overview of the experimental setup used to investigate mesophase formation during the electrode capture process. Experiments were performed under both reflected illumination and by observing transmitted light through crossed polarizers using optically transparent electrodes..... 50
Figure 21	Schematic illustration of cholesteric organization in double-stranded DNA..... 53
Figure 22	Schematic representation of the effect of incident light scattering and refractive index changes occurring at the surface of the capture electrode..... 56
Figure 23	Proof of concept for label-free protein detection. Egg white lysozyme protein (4% w/v in 1x TBE buffer) is concentrated at an electrode surface (50 $\mu\text{m}$ wide) by performing a dual focus with $\sim 2.5$ V potential..... 59
Figure 24	Buffer exchange ..... 62
Figure 25	Stress acting on the surface of electrodes due to flow of buffer in the microchannel (50 $\mu\text{m}$ x300 $\mu\text{m}$ cross section channel)..... 63

	Page
Figure 26	The capture-release chip is attached to an FPGA board that is connected and programmed through a USB cable using a Personal Computer..... 66
Figure 27	Top level block diagram of the FPGA based portable analysis device showing flow of information and electrical signalling..... 67
Figure 28	Software and hardware components of the portable device programming and their communication channels ..... 68
Figure 29	Screenshots of USB communication initialization window and the capture-release window showing the user input for the time of each capture and the number of capture-release steps to be taken.... 70
Figure 30	The Use Case diagram with details of each step ..... 71
Figure 31	Applicability of the Capture-Release electrode array to multiple on-chip operations described in this work ..... 74

## LIST OF TABLES

		Page
Table 1	Sample injection techniques in microfabricated devices.....	7
Table 2	Characteristic species parameter values used in simulation studies..	40
Table 3	The values of wire bonding parameters that were found to work well for the bonding of PCB and gold electrodes on silicon devices	95

## CHAPTER I

### INTRODUCTION

Microfabricated lab-on-a-chip systems are inexpensive devices as they exploit the cost cutting advantages of microfabrication. When used for bioanalytical and biosensing applications these offer an unprecedented level of speed and portability, putting the power to conduct increasingly complex and sophisticated tests directly into the hands of those who need it (doctors, soldiers, criminologists, etc.). The need for pre-existing laboratory infrastructure, trained lab-technicians to perform the tests and funds to cover the cost of the test is undermined with this technology. In addition to enhancing the cost savings per test, the small nanoliter amounts of the sample and reagents used in these devices make them an environmentally conscious choice. Physics and chemistry knowledge of the relevant processes and engineering principles are applied in designing efficient strategies to handle the various on-chip components required for these tests.

Microdevices continue to be developed to perform a variety of bioanalysis assays, however many of these deal with such minute amounts of charged biomolecules (DNA, proteins and peptides) that they must first be concentrated to a detectable level. After preconcentration, the biomolecules generally need to be purified and injected into another region of the chip. Efficient strategies for precisely handling minute amounts of charged biomolecules in microchannel geometries are critically needed. The sequential

---

This dissertation follows the style of *Proceedings of the National Academy of Sciences of the United States of America*.

steps generally carried out after sample preparation, for on-chip bioanalysis are outlined as follows:

Sample purification → Concentration → Focusing → Injection → Analysis, Detection

All these steps are generally designed to be carried out in separate on-chip locations. Efficient techniques have been proposed that achieve each of the steps individually. The main challenge has been to integrate these steps on a single analysis chip, so as to get sample-to-results on the same chip. Chip design would be simplified greatly if more than one analysis step could be achieved using the same technique and furthermore, at the same on-chip location. This would also result in a device with a smaller footprint. In addition, integration of lesser on-chip components would then be required to design a sample-to-results chip.

In order to address this need, the current work was undertaken to investigate the use of an array of microfabricated electrodes to achieve the steps of *pre-concentration and focusing of DNA inside microchannels, purification of the concentrated sample, and its injection into an analysis channel*. By applying a low voltage (~1-2V) between neighboring electrodes positioned within a microchannel, DNA fragments being intrinsically negative polyanions, are induced to move toward and collect at the anode. This also allows the amount of DNA to be metered using an array of electrodes. The research achieved the following objectives:

1. DNA sample concentration, focusing, metering and injection in microchannels.
2. Switching or exchanging the suspension buffer for analyte purification.

3. Development of a portable PC-programmable prototype device for concentration of DNA.

The successful completion of these objectives has demonstrated the efficiency and robustness of this sample processing technique in working with different analytes in a range of ionic environments while carrying out multiple bioanalysis operations, and the ease in its integration with portable programmable electronics to enable truly portable and integrated lab-on-a-chip bioanalysis systems in the future. In addition to achieving these objectives, an interesting *visible light scattering effect* was observed on top of the microfabricated electrodes when DNA or proteins are collected and compacted on them. This could be used as a simplistic and sensitive *label-free detection technique*. The phenomenon is reversible and the captured biomolecules can be resuspended back into the buffer on switching off the voltage.

## CHAPTER II

### DNA CONCENTRATION AND FOCUSING IN MICROCHANNELS

#### 2.1 Background

On the macroscale, conventional techniques to increase the concentration of charged biomolecules typically involve the use of either physical processes (e.g., centrifugation) or chemical amplification via the polymerase chain reaction (PCR). Centrifugation is generally difficult to miniaturize and interface with other microfluidic components, while PCR techniques are not straightforward to apply when the sample of interest contains multiple components or is unknown. In addition, PCR products contain enzymes, primer oligonucleotides, and other chemical species in addition to the target DNA of interest; often making it is necessary to incorporate additional purification steps prior to subsequent analysis.

In addition to an increase in concentration, many bioassays also benefit greatly from the ability to *focus* the sample by restricting its occupied volume. The design of miniaturized systems for performing size selective fractionation of DNA using gel electrophoresis, for example, illustrates the critical importance of sample focusing. Here, the ability to distinguish or *resolve* spatially distinct zones containing like-sized DNA fragments is determined through an interplay between the relative migration velocities of neighboring zones and the rate at which the zones broaden due to the combined effects of molecular diffusion and electric field mediated dispersion.



Separation resolution increases with the relative migration velocity and with the overall length of the separation channel, but decreases with the injected zone width and the magnitude of the longitudinal dispersion coefficient (1). Operation in a miniaturized format dictates that the overall device length be minimized, thereby making the injected zone width the most straightforward parameter to manipulate since all other factors depend on properties specific to particular analyte and sieving matrix formulations. These considerations point to the need for broadly applicable techniques to achieve *simultaneous concentration and focusing* in microfluidic DNA analysis systems.

## 2.2 Literature

Conventional electrokinetic injection techniques typically require the use of off-chip electrodes with potentials in the 1–2 kV range—requirements that are not straightforwardly transferable to a compact and portable microdevice format. For example, a variety of electrokinetic sample injection schemes have been developed based on the so-called *T-injector* arrangement (2), wherein separate injection and separation microchannels intersect to form a ‘T’ shaped geometry. In this configuration, sample injection is achieved by differential application of electric potential differences between the injection and separation channels. Subsequent refinements include the *cross* (3, 4) and *double-T* (5) designs that offer greater control over the size of the injected zone. In addition to geometry, the electric field in the vicinity of the channel intersection can also be manipulated (*pinched* injection) in order to further define the injected zone size and shape (6). Other variations on the basic T-injector configuration

involve the incorporation of microporous (7) and nanoporous (8) membranes, thin film electrodes (9), optical gating (10, 11), and locally narrow channel geometries (12). Stacking at the interface between the sample and a background buffer has also been performed in T-injector geometries (13-17). Other techniques investigated include employing bulk flow (18), capillary (19), diffusion-based (20), pressure-driven (21), hydrodynamic (22), and dielectrophoretic trapping (23-25) processes. The use of nanocapillary array interconnects (26), as well as designs exploiting opposing electrophoretic and electroosmotic processes in the vicinity of a microchannel-nanochannel intersection (27, 28) have also been explored to achieve concentration of DNA and proteins. All these techniques are broadly summarized in Table 1.

The concept of using on-chip electrodes to achieve directed migration of oligonucleotide fragments in microfluidic devices has been recognized in the context of DNA microarrays (29-31). Using microelectronic array technology, assemblies of addressable electrodes have been designed to transport samples to particular locations on an array surface in order to enhance hybridization efficiency, with specificity enhanced by post-hybridization reversal of the electric field (32). The ability to use electrodes positioned inside a microchannel to focus DNA samples prior to injection into an electrophoresis gel has also been demonstrated (33). More recent work has shown that placement of on-chip electrodes within an electrophoresis microchannel can, with proper design, enable selective extraction of fractionated bands from the gel for subsequent analysis (34, 35). These advances suggest the possibility of configuring on-chip

Table 1. Sample injection techniques in microfabricated device.


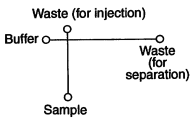
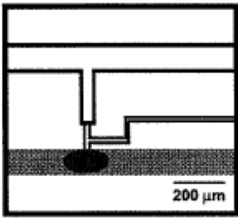
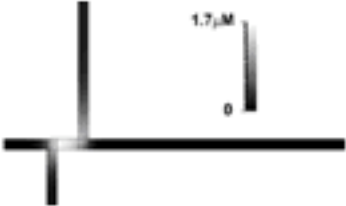
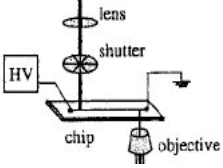

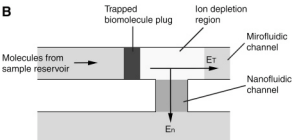
Description	Schematic	Compaction (Y/N)	Focusing (Y/N)	Concentration Enhancement	Voltage (V)	Reference	Comments
Capture-release / electrode array		Y	Y	50X	1	This work	No electrokinetic bias, buffer exchange possible
Electrokinetic, intersecting channels		N	Y (pinched injection)	None	500–2000	(2) (3) (6) (12)	Intersecting channel geometry defines injection volume
Hydrodynamic / pressure driven		N	N	None	--	(21) (22)	No electrokinetic bias, pressure source needed (17)
Stacking / ITP		Y	Y	3.9–13X	480–500	(15) (16)	Different sample and background buffers needed
Optical gating		N	Y	None	--	(10)	Serial injections possible

Table 1 Continued.

Description	Schematic	Compaction (Y/N)	Focusing (Y/N)	Concentration Enhancement	Voltage (V)	Reference	Comments
Microfabricated membrane / Nanocapillary array inter-connects		Y	N	30–90X	1100–3000	((7) ((8))	Nanocapillary array and nanoporous polyester membrane
Electrokinetic trapping by nanofluidic filters		Y	N	$10^6$ - $10^8$ X	10-30V	((28))	Timescales for concentrating is in hours

electrode arrays to efficiently achieve *simultaneous concentration and focusing* of charged analytes in microfluidic systems.

### **2.3 The Capture-Release Approach**

In the current work, an array of electrodes is used to sequentially capture and subsequently release the DNA lying between neighboring electrodes. If we number the electrodes in the array with increasing number signifying the sequence that particular electrode is activated. Initially #1 is cathode and #2 is anode with a low applied voltage of approximately 1 V (Fig. 1). Being a polyanion, practically all of the DNA lying between these two electrodes migrates electrophoretically to the anodic electrode (#2). Now the anodic potential is switched to the next electrode in the array (#3). The DNA lying between the #2 and #3 electrodes now moves to the #3 electrode in which is the new anode. In addition to the DNA between the new pair of electrodes, the DNA that was captured on top of the #2 electrode also migrates electrophoretically to the new anode. This effectively sweeps the DNA originally lying between #1, #2 and #3 electrodes to the surface of the #3 electrode as evidenced by the loss of fluorescence between then relative to the rest of the microchannel (Fig. 1D). This process can be repeated multiple times using subsequent electrodes in the array to achieve higher concentrations of the collected DNA.

The DNA plug formed on the anode is focused as it assumes the shape and size of the anode. This results in simultaneous concentration and focusing of the DNA

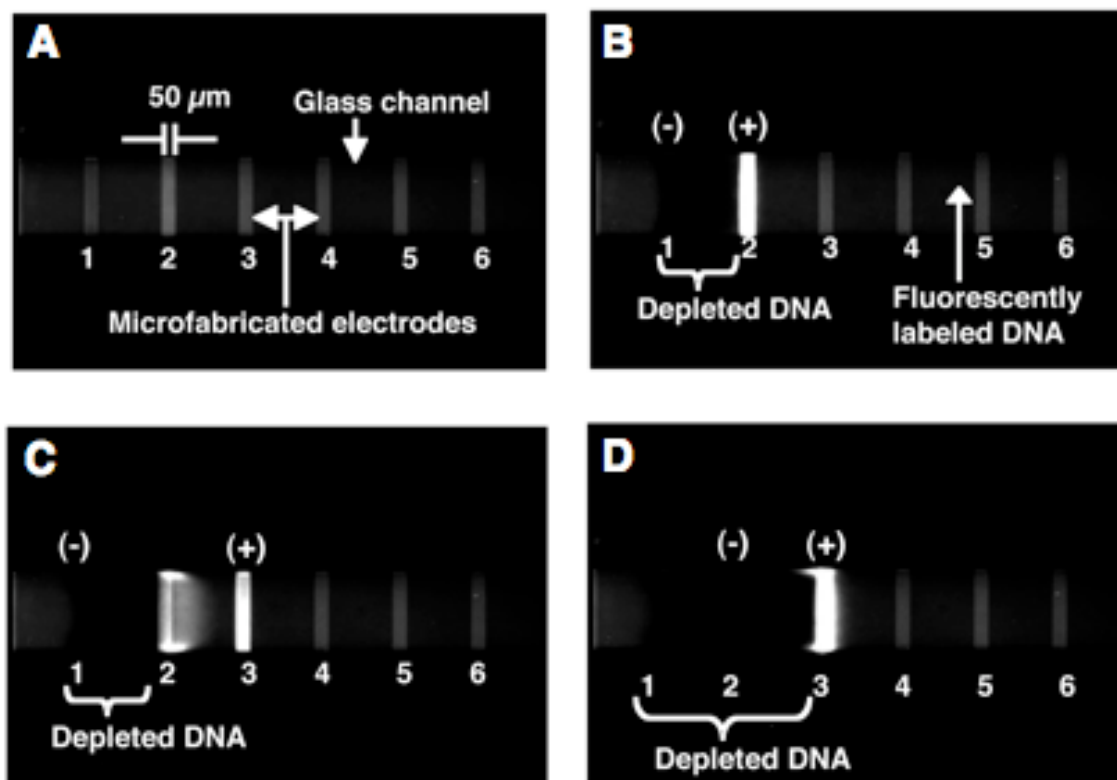


Figure 1. Simultaneous concentration and focusing of DNA using an array of individually addressable microelectrodes. (A) Image of the electrode array within the device (channel dimensions are 275  $\mu\text{m}$  wide by 45  $\mu\text{m}$  tall, electrodes are 50  $\mu\text{m}$  wide with a 225  $\mu\text{m}$  edge-to-edge spacing). A 100 bp dsDNA ladder (12  $\mu\text{g}/\text{ml}$  in 1x TBE buffer with 10% v/v BME) fluorescently labeled with YOYO-1 intercalating dye is loaded inside the microchannel. (B) A potential of 1 V is applied to the first two electrodes in the array resulting in migration toward the anode (electrode #2) of DNA initially between the two electrodes, after which it becomes ‘captured’ at the anode (migration is from left to right). (C) The anodic potential is switched to electrode #3 while the cathodic potential is switched to electrode #2 resulting in release of the captured DNA and migration toward electrode #3. (D) DNA initially between electrodes #1 and #3 becomes captured at electrode #3. This process is repeated until a desired concentration is achieved.

sample. The magnitude of concentration achieved in different relevant buffer environments and electrode metals are similar (Fig. 2) and thus the process can be termed as robust of a range of different environments. The concentrated and focused

DNA plug can now be used in a variety of applications, some of which are covered in the following sections. The intensity increases should not be linearly correlated with increases in concentration as it is expected that due to compaction of the DNA very close to the electrode will lead to fluorescence-quenching resulting in a decrease in the observed fluorescence intensity. In effect, the fluorescence intensity would not scale linearly with increases in DNA concentration at the capture electrode.

#### **2.4 Dual Focus and Metering**

The width of the captured sample zone can be further reduced by imposing a *dual focusing* scheme whereby a negative potential is applied to both electrodes located on either side of the capture anode (Fig. 2). This process can be applied either at each individual capture step or at the final electrode position, and ensures that the captured DNA remains tightly confined in the vicinity of the electrode surface. Using the combined electrode capture and dual focusing process, a 50-fold increase in DNA concentration is achieved over a downstream distance of 3.9 mm (Fig. 3). Additionally, dual focusing can be simultaneously applied to multiple electrodes in the array to generate metered amounts of DNA at a number of anodes (Fig. 4) in order, for example, to enable discrete serial injections to be directed into a network of analysis channels. With the equispaced electrodes in the array we get equal amounts of DNA on the electrodes that could enable multiple serial injection of the same amount of analyte, in the same or multiple channels. Amounts captured can be further manipulated by adjusting the inter-electrode spacing, electrode size, and the applied voltage level.

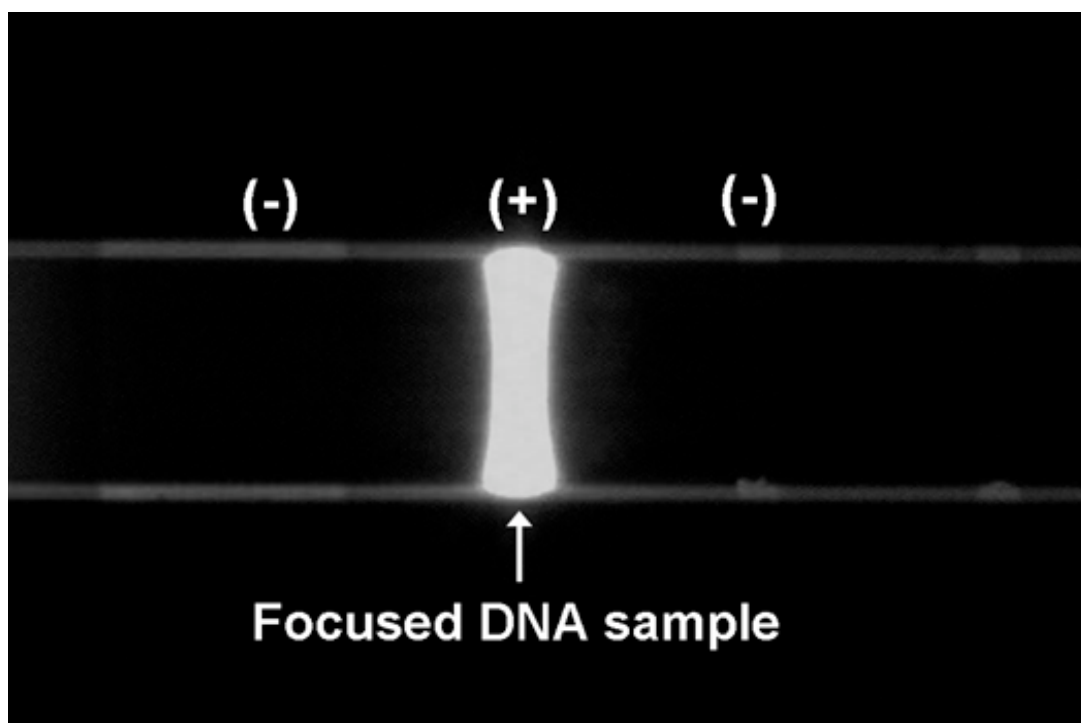


Figure 2. Snapshot of the capture of DNA showing the dual focus applied by applying opposing electric field on both sides of the capture electrode leading to the highly focused DNA plug. A potential of 1V is applied to the focusing electrodes shown in this figure.



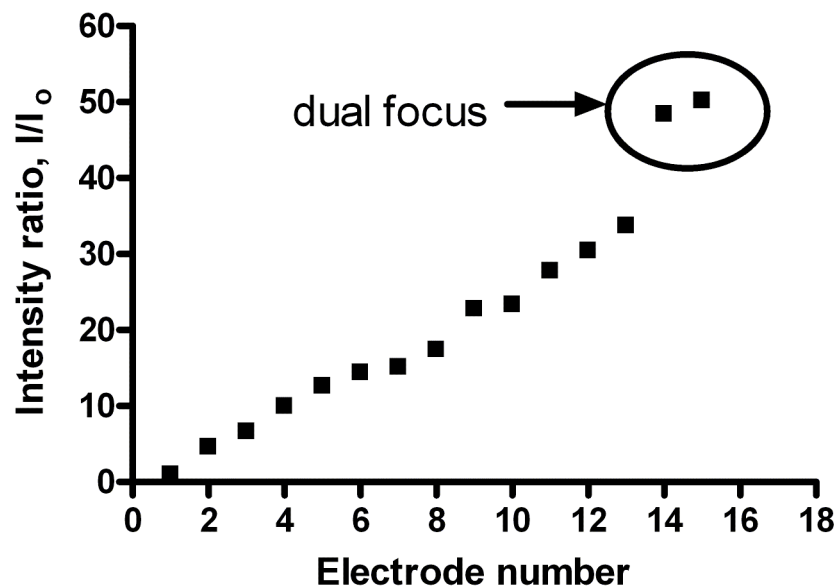


Figure 3. The increase in concentration at each subsequent electrode in the array is indicated by increases in the detected normalized fluorescence intensity. The higher intensity recorded at the last two electrodes relative to the trend in the earlier electrodes, is a result of a dual focusing voltage that restricts the DNA almost completely on top of the electrode which is the defined detector area in image analysis.

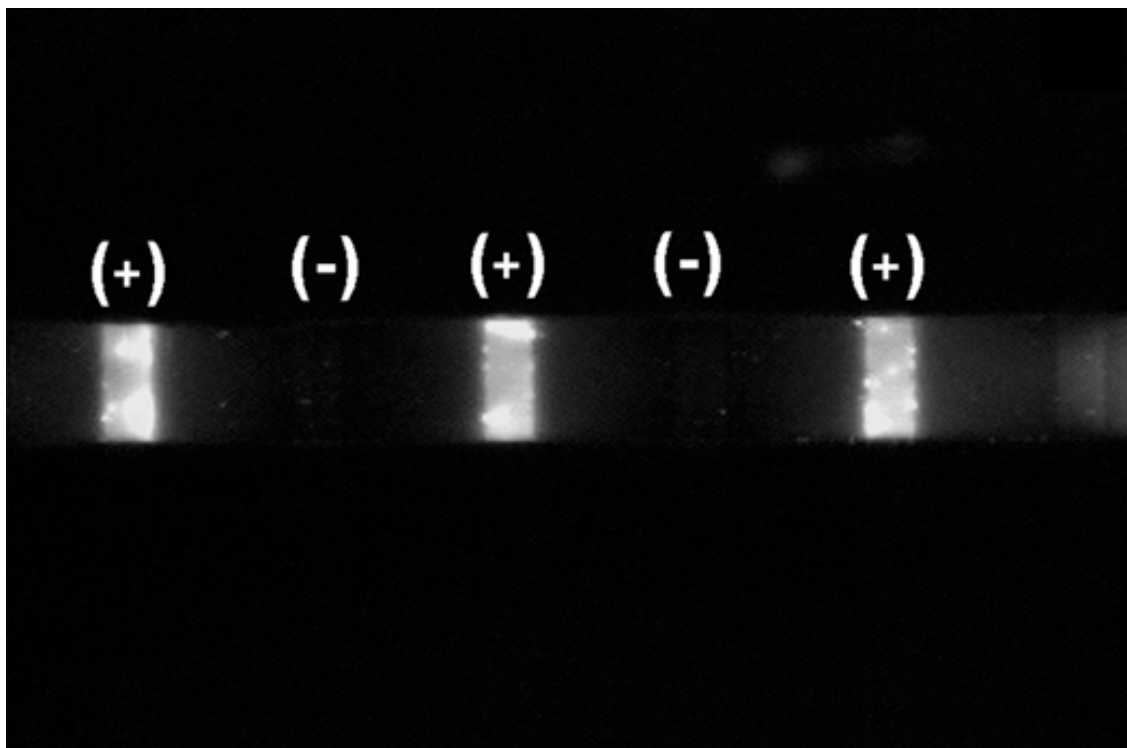


Figure 4. Metering of DNA sample achieved by simultaneously applying the dual focus at a number of neighboring electrodes. This provide additional functionality for discrete multiple injection into the same or multiple analysis channel. The amount of DNA at each electrode is primarily governed by the channel geometry and spacing between the electrodes.

## 2.5 Characterization and Analysis

By fluorescently labeling the DNA sample, it is possible to observe discrete stepwise increases in fluorescence intensity that correspond to discrete increases in concentration occurring during the capture process. Image analysis is used to extract intensity data at the surface of each electrode, which can then be converted to concentration via a calibration curve. DNA concentration scales linearly with the number of electrodes in the array for a constant inter-electrode spacing, and the efficiency of the capture-release process is robust over a range of ionic conditions

relevant in molecular biological applications (Fig. 5). Furthermore, neither the amount of the anti-photobleaching agent  $\beta$ -mercaptoethanol (BME) added nor the use of different electrode materials significantly impacts the achievable concentration level. The capture-release process is effective for both single- and double-stranded DNA, although kinetics are somewhat accelerated for double stranded species.

The ionic environment in which the DNA fragments are suspended does, however, influence the kinetics of the capture process. This was characterized by monitoring the increase in fluorescence at the anode as a function of time during the capture process and fitting the data to a one parameter exponential equation:  $y = 1 - \exp(-t/\tau)$ . Here,  $y$  is the normalized intensity of the collected DNA,  $t$  is the time in seconds, and  $\tau$  is a characteristic time constant. This analysis indicates that the kinetics of the capture process are significantly faster in histidine buffer than those observed with the same DNA sample suspended in TBE. Furthermore, these data indicate that the presence of BME accelerates the capture kinetics in TBE buffer, possibly through the creation of a more favorable ionic environment through its activity as a free radical scavenger. The degree of acceleration is most pronounced at low TBE concentrations ( $0.5\times$  and  $1\times$ ) as was expected, and becomes largely insensitive to BME concentration once the quantity added to the sample exceeds a threshold value. Addition of BME to histidine buffer, however, does not significantly alter capture kinetics.

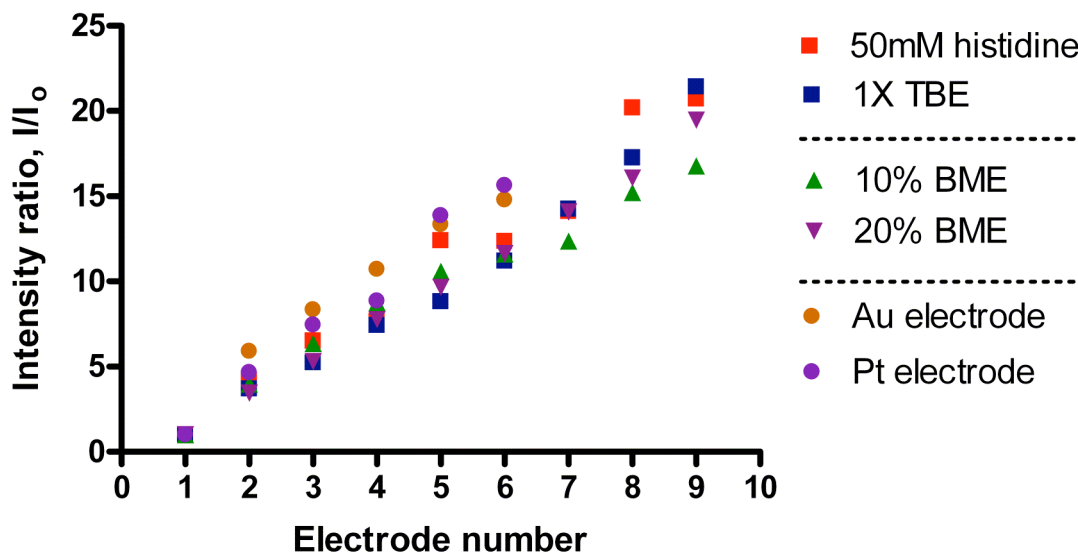


Figure 5. The achievable concentration as indicated by normalized level of fluorescence intensity is robust and essentially independent of buffer composition, amount of BME, and electrode material.

The underlying physics associated with the electrode capture process can be better understood by considering the relative influence of electrophoretic and electroosmotic effects. An estimate of a characteristic electrophoretic migration velocity can be obtained from the free solution mobility of double-stranded DNA ( $\mu_0 \sim 4.5 \times 10^{-4} \text{ cm}^2/\text{V}\cdot\text{s}$  in TBE buffer (36)) and the electric field strength ( $E \sim 40 \text{ V/cm}$ ), yielding a velocity of  $u_{EP} = \mu_0 \cdot E \sim 180 \text{ }\mu\text{m/s}$ . While this calculation is not expected to provide an exact representation of the observed migration velocities owing to the range of different buffer compositions studied, it nevertheless provides a useful order of magnitude estimate.

In order to characterize the influence of electroosmosis, two interrelated factors must be considered. First, we note that electrode capture process is performed in a sealed environment in order to prevent evaporation, which otherwise exerts an overwhelming effect on the flow within the microchannel. This sealed arrangement confines the liquid within a fixed volume thereby presenting a considerable mechanical resistance to bulk flow as a consequence of fluid incompressibility. Secondly, electroosmotic pumping is localized between the active electrode pair inside the microchannel, in contrast to the more conventional configuration where an electric field is applied across the entire channel length. In this case of localized electroosmosis, the balance between hydrodynamic effects inside and outside the actively pumped region results in a scaling of pumping velocity with *applied potential* between electrodes rather than electric field strength (37). An estimate of the characteristic electroosmotic velocity can then be obtained from  $u_{EOF} = \epsilon\epsilon_0\xi V/\eta L$ , where  $\epsilon$  is the dielectric constant of the buffer solution,  $\epsilon_0$  is the permittivity of free space,  $\xi$  is the zeta-potential of the buffer solution,  $V$  is the applied potential,  $\eta$  is the fluid viscosity, and  $L$  is the entire length of the microchannel from inlet to outlet. Assuming characteristic material properties for water at room temperature,  $\xi = 100$  mV for the silicon/glass surfaces (38, 39), a 1 V potential, and  $L = 3.1$  cm, yields a value of  $u_{EOF} \sim 2.3$   $\mu\text{m/s}$ . Not only is this nearly two orders of magnitude smaller than  $u_{EP}$ , the calculation is based on an open channel configuration and is thus expected to represent an idealized upper limit to the actual  $u_{EOF}$  achievable in the sealed arrangement. Flow visualization studies using carboxylated polystyrene

microsphere tracers further confirm the absence of bulk electroosmotic flow under conditions associated with the electrode capture process.

## CHAPTER III

### DNA INJECTION INTO MICROCHANNELS

DNA or other biomolecules are routinely required to be injected into a microchannel or a region on the microfabricated analysis chip for sample preparation, certain biochemical reactions like PCR or analytical techniques like gel-electrophoresis.

#### **3.1 Background and Significance**

One of the major advantages of working at the microscale is that only minute amounts sample or analyte are required. Though this has many advantages as outlined earlier, the handling of such minute amounts of analyte can be challenging. For example, the analytical process that is being miniaturized may require the analyte to be restricted to a particular location in the microchannel for a certain amount of time. Electrophoresis of DNA fragments in a gel (size selective fractionation of DNA) is a common analysis technique and a suitable one to demonstrate the critical importance of pre-concentration and focusing of the sample analyte plug prior to injection into a microchannel for analysis.

#### **3.2 Capture-Release Injection**

In electrophoresis, the ability to distinguish or *resolve* spatially distinct zones containing like-sized DNA fragments is determined through an interplay between the relative migration velocities of neighboring zones and the rate at which the zones

broaden due to the combined effects of molecular diffusion and electric field mediated dispersion. A resolution parameter  $R$  is often defined (1) in terms of a ratio of the separation distance between neighboring zones relative to their width, which, when expressed in terms of observable parameters yields:

$$R = \frac{1}{4} \left( \frac{\Delta\mu}{\mu} \right) \frac{L}{\sqrt{\sigma_{inj}^2 + \sigma_{det}^2 + 2D^E \left( \frac{L}{\mu E} \right)}} \quad (1)$$

In this expression,  $\mu$  is mobility associated with each zone,  $\Delta\mu/\mu$  is the selectivity (a parameter characterizing relative mobilities between neighboring zones of different length),  $L$  is the effective separation length (the distance between the injection and detection points),  $\sigma_{inj}^2$  is the variance (i.e., width) of the injected sample plug,  $\sigma_{det}^2$  is the variance introduced due to the finite detector size, and  $D^E$  is longitudinal dispersion coefficient of the DNA fragments in the gel (the superscript  $E$  denotes an electric field dependence).

Equation (1) illustrates the mechanism by which separation resolution increases with the selectivity and the length of the separation channel, but decreases with the injected plug width and dispersion. Operation in a miniaturized format dictates that  $L$  be minimized, thereby making injection width  $\sigma_{inj}^2$  the most straightforward parameter to manipulate since all other factors depend on the properties specific to particular analyte and sieving matrix formulations. Moreover, although  $\sigma_{det}^2$  can be reduced by employing a narrow detection window, the corresponding reduction in signal amplitude must be offset by use of more concentrated samples. These considerations point to the need for



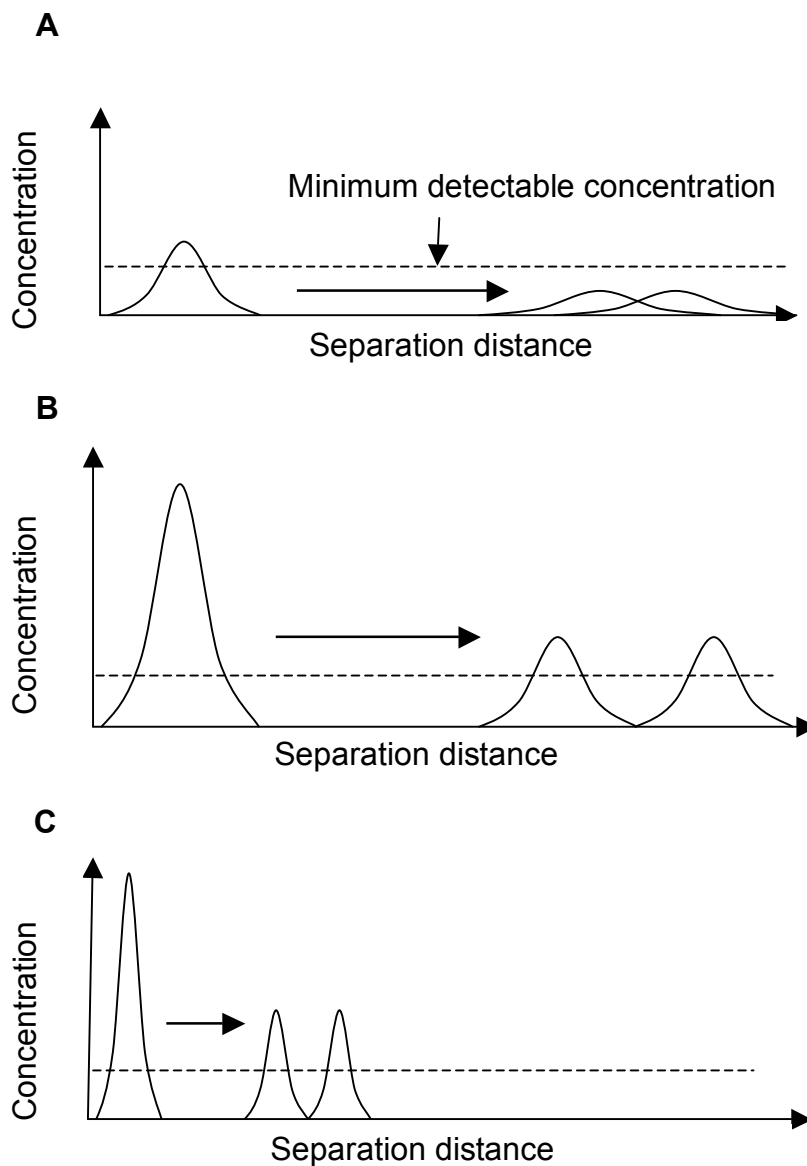


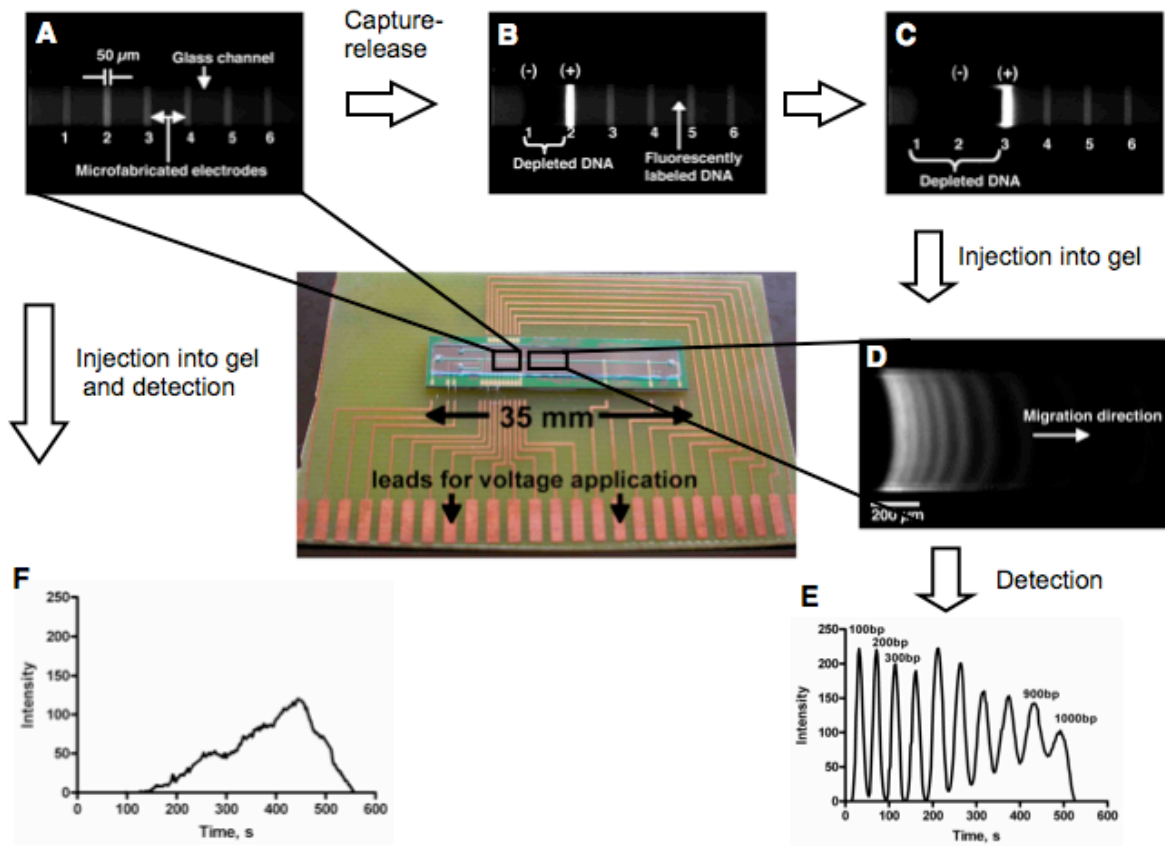
Figure 6. The influence of focusing and concentration of an injected sample on the ability to detect and resolve two distinct components by electrophoretic separation. (A) Injection of a *non-concentrated and unfocused* sample zone requires a long separation distance in order to distinguish each component, however the corresponding signal from each species falls below the detectable range as the zones spread by diffusion and dispersion during the time elapsed while traveling this distance. (B) Injection of a *concentrated but unfocused* sample zone allows each component to be detected, but a long separation distance is still required. (C) Injection of a *concentrated and focused* sample zone allows each component to be detected more rapidly because a considerably shorter separation distance is required.

broadly applicable techniques to achieve simultaneous concentration *and* focusing in microfluidic DNA analysis systems (Fig. 6).

### **3.3 Enhanced Electrophoresis Resolution on Microfabricated Chip**

After a sufficient number of capture-release cycles have been performed to raise the concentration to a desired level, the resulting highly focused and concentrated sample can be dispensed or injected into an analysis channel for subsequent analysis. The utility of this scheme is illustrated by employing it to achieve enhanced sensitivity in microchip-based gel electrophoresis of DNA at concentrations that are initially below a detectable level (Fig. 7A). After a sequential capture-release process has been completed (Fig. 7B-C), the sample is injected into the gel by simply switching the applied potential to a set of on-chip electrodes spanning the analysis portion of the microchannel. This focusing process allows all bands in a fluorescently labeled double-stranded DNA ladder to be resolved within a distance of 3 mm from the gel interface (Fig. 7D-E), whereas the fragments are not easily resolvable in an identical sample that was not pre-concentrated by the capture-release process (Fig. 7F).

Figure 7. Effect of the pre-concentration and focusing process on the separation resolution. (A) Image of the electrode array within the device. Channel dimensions are 275  $\mu\text{m}$  wide by 45  $\mu\text{m}$  tall, and electrodes are 50  $\mu\text{m}$  wide with 225  $\mu\text{m}$  edge-to-edge spacing. A 100-bp double-stranded DNA ladder [12  $\mu\text{g}/\text{ml}$  in 1 $\times$  TBE buffer with 10% (vol/vol) BME] fluorescently labeled with YOYO-1 intercalating dye is loaded inside the microchannel. (B) A potential of 1 V is applied to the first two electrodes in the array, resulting in migration toward the anode (electrode 2) of DNA initially between the two electrodes, after which it becomes captured at the anode (migration is from left to right). The anodic potential is now switched to electrode 3, resulting in release of the captured DNA. The cathodic potential is switched to electrode 2, and migration continues toward electrode 3 until all DNA initially between electrodes 1 and 3 becomes captured at electrode 3(C). This process is repeated until a desired amount of enrichment is achieved. (D) Electrophoretic separation of a 100-bp double-stranded DNA ladder sample initially at 6  $\mu\text{g}/\text{ml}$  [1 $\times$  TBE buffer with 10% (vol/vol) BME] after concentration and injection into a gel matrix photopolymerized inside the microchannel immediately downstream of the final electrode in the capture array (5% T-crosslinked polyacrylamide gel, Electric field=23 V/cm). (E) All fragments in the DNA ladder are resolved in a separation length of 3 mm. (F) Without focusing and concentration before injection into the gel, fragments are unresolvable at the same separation length. The total area under the peaks in E is approximately double that in F, as expected because the quantity of focused and concentrated DNA injected in the separation of E was nearly double that in the unfocused separation of F (based on the initial sample concentration and volume contained between electrodes in each case).



## CHAPTER IV

### DEVICE DESIGN AND OPERATION

#### 4.1 Device Components

Microfluidic chips were constructed by bonding etched glass microchannels to silicon substrates patterned with arrays of individually addressable microfabricated electrodes (Figs. 8 and 9). The inter-electrode spacing within the array (225  $\mu\text{m}$  edge-to-edge) allows modest electric fields ( $\sim 40$  V/cm) to be achieved with a minimal applied potential (1 V). Under these conditions, a sufficient electrostatic driving force is developed to direct DNA migration while maintaining a voltage below the threshold for bubble formation arising from hydrolysis reactions at the electrode surfaces (30, 31). First, a DNA sample is loaded into the microchannel using a syringe, after which the access holes are sealed with adhesive tape to prevent evaporation. The chip is now ready to be experimented with. The capture-release experiments are conducted using the sample loaded chip. Once the experiment is over, the adhesive tape is removed from the access holes and the sample is removed using a vacuum pump. The channel is then rinsed with DI water, dried with air using the vacuum pump and inspected under a microscope to check for any electrode or channel fouling.

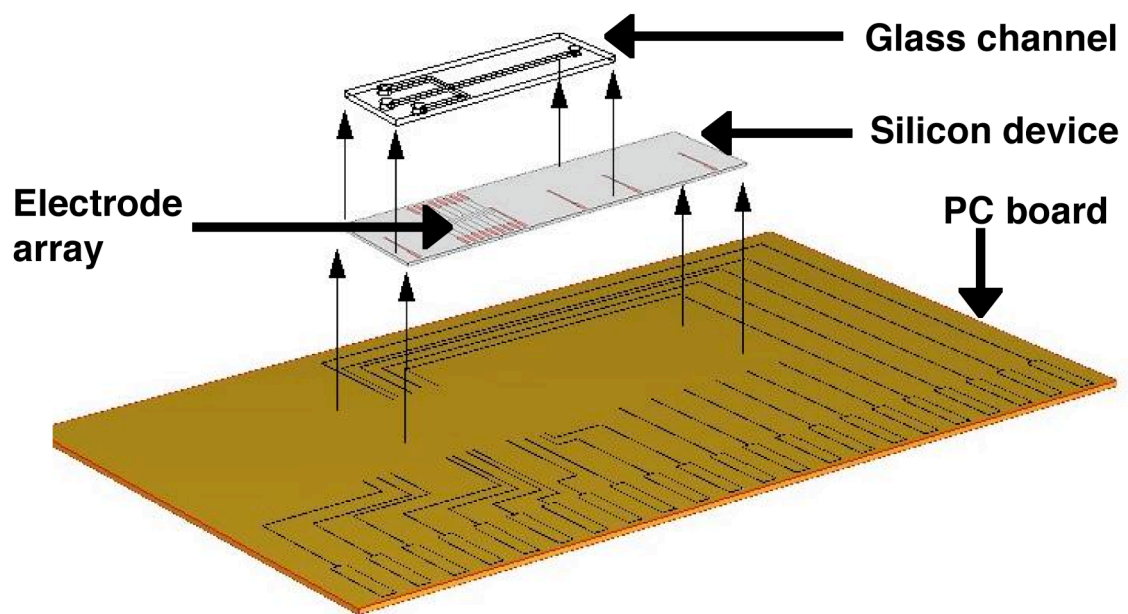


Figure 8. Exploded view of the capture-release chip showing device components.

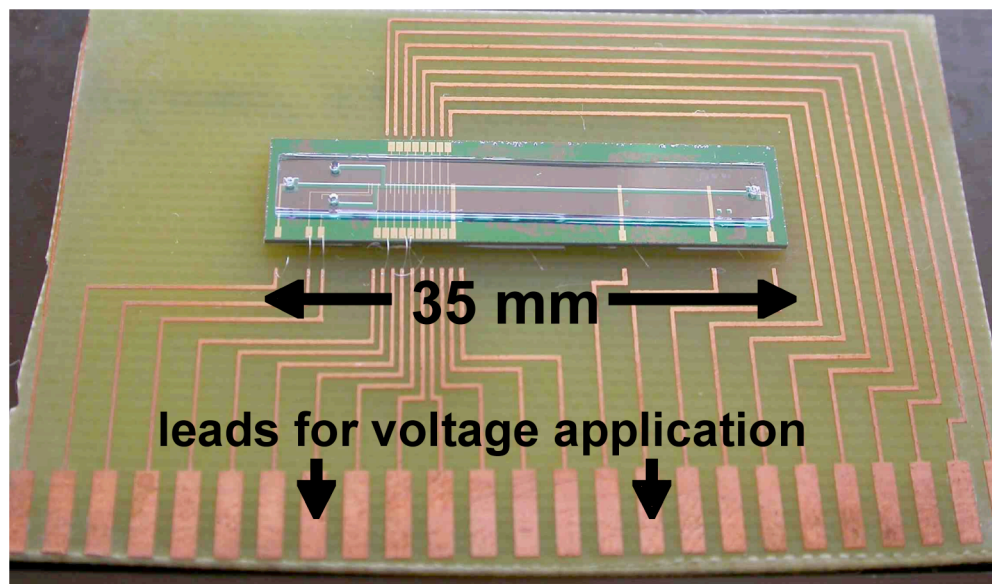


Figure 9. Assembled capture-release chip showing the electrode array.

## 4.2 Microchip Fabrication and Assembly

The electrode array chips consist of three components: a silicon device ( $\sim 7.5 \text{ mm} \times 35 \text{ mm}$ ), a glass microchannel ( $\sim 3.9 \text{ mm} \times 33.5 \text{ mm}$ ), and a printed circuit (PC) board ( $\sim 4 \text{ cm} \times 6.4 \text{ cm}$ ) as shown in Figs. 7-8. Silicon wafers ( $500 \text{ }\mu\text{m}$  thick,  $150 \text{ mm}$  diameter,  $\langle 100 \rangle$ , with a  $5000 \text{ }\text{\AA}$  thick oxide layer (University Wafer)) were cleaned using a reactive ion etcher, spin coated with hexamethyldisilazane (J.T. Baker) and positive photoresist SPR 220-7.0 (Rohm and Haas Electronic Materials LLC), patterned, and developed using MF-319 developer (Rohm and Haas Electronic Materials LLC). Gold electrodes were fabricated by depositing a  $500 \text{ }\text{\AA}$  layer of chromium followed by a  $1000 \text{ }\text{\AA}$  layer of gold using a thermal evaporator (Fig. 10), while platinum electrodes were fabricated by depositing a  $500 \text{ }\text{\AA}$  layer of titanium followed by a  $1000 \text{ }\text{\AA}$  layer of platinum using an electron beam evaporator. Glass microchannels were fabricated by depositing a  $600 \text{ }\text{\AA}$  chromium layer followed by a  $4000 \text{ }\text{\AA}$  gold layer on glass wafers (borofloat,  $500 \text{ }\mu\text{m}$  thick,  $150 \text{ mm}$  diameter, (Precision Glass & Optics)) that had been cleaned using a reactive ion etcher. The wafers were then spin coated with positive photoresist SPR 220-7.0, patterned, developed using MF-319, and hard baked. After immersion for 10 minutes each in gold etchant (Transene Co.) and chromium etchant (Cyantek Inc.), the exposed glass was then etched using a freshly prepared 7:3 v/v solution of hydrofluoric and nitric acids (etch rate  $\sim 5 \text{ }\mu\text{m}/\text{minute}$ ) to a channel depth of  $45 \text{ }\mu\text{m}$  (width =  $275 \text{ }\mu\text{m}$ ). After dicing, fluidic access holes were drilled using an electrochemical discharge process. Silicon devices were mounted on PC boards and wire bonded to provide electrical connections (Fig 11). The wire bonds were



encapsulated with epoxy for protection (Fig. 12). Glass microchannels were then bonded to the silicon device using a UV curable optical adhesive (SK-9 Lens Bond; Summers Laboratories).

### **4.3 Preparation of DNA Samples**

Electrode capture experiments were carried out using a 100 base pair double-stranded DNA ladder (Bio-Rad Laboratories, Inc.). The DNA ladder was suspended in tris-borate-EDTA (TBE) (Bio-Rad Laboratories, Inc.) and histidine (Sigma-Aldrich Co.) buffers. An intercalating dye (YOYO-1; Invitrogen/Molecular Probes) was used to fluorescently label the DNA, and  $\beta$ -mercaptoethanol (Sigma-Aldrich Co.) was added to inhibit photobleaching (intensity measurements were calibrated to account for residual photobleaching). 10  $\mu$ l master mixes of fluorescently labeled DNA samples were prepared by adding the as-supplied DNA ladder solution to 1 mM YOYO-1 intercalating dye in a 2:1 v/v ratio. After incubation for several minutes at room temperature, the suspension buffer was extracted using a vacuum centrifuge evaporator. The sample was then re-suspended in the appropriate buffer system and the desired amount of  $\beta$ -mercaptoethanol was added. This procedure allowed preparation of serial dilutions of DNA concentration while preserving consistent fluorescent dye loading conditions.

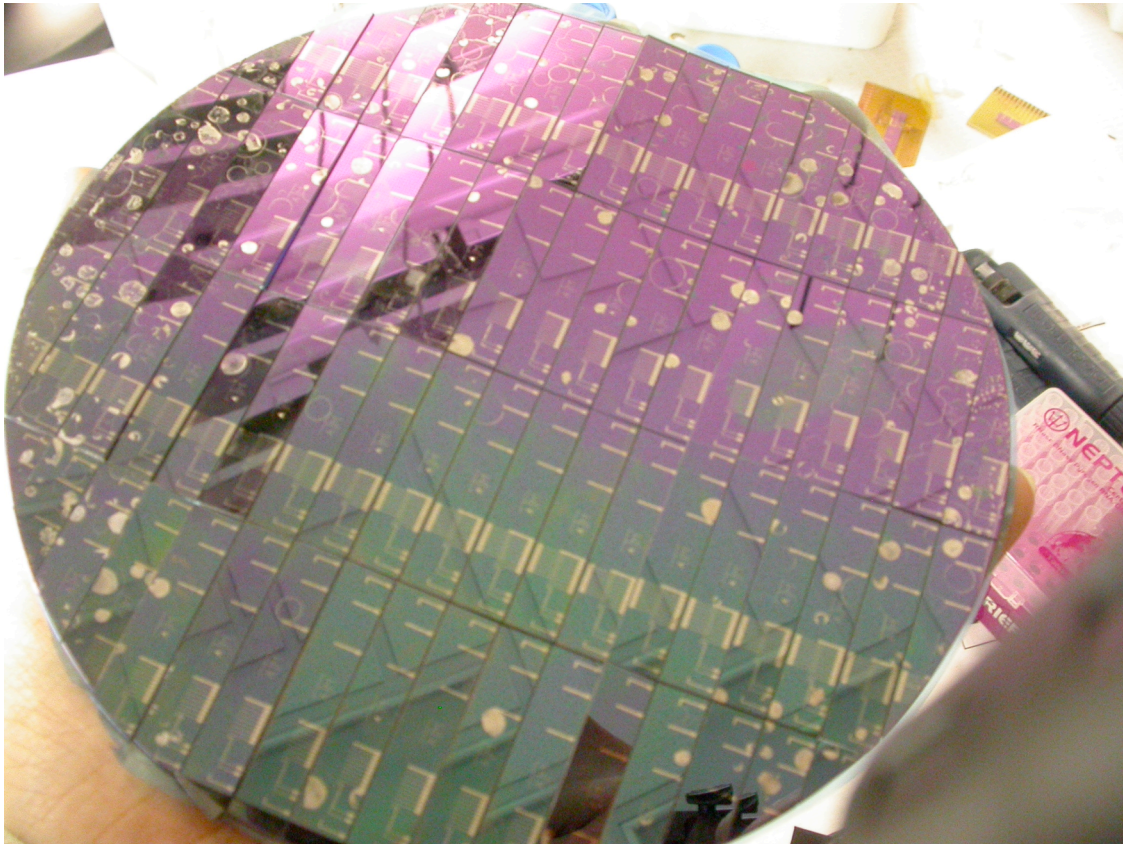


Figure 10. A 6 inch silicon wafer after lithography, gold deposition and dicing.

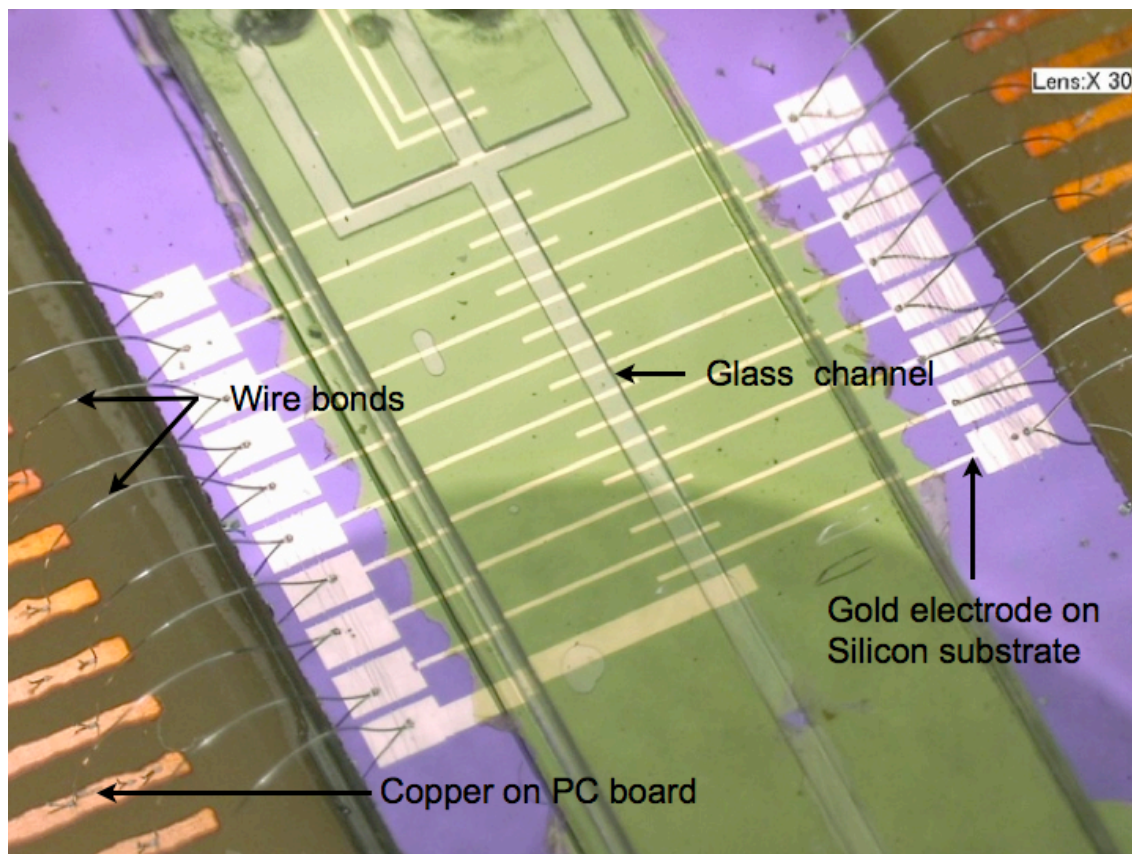


Figure 11. A close up image of the capture-release device revealing the assembly of various components.

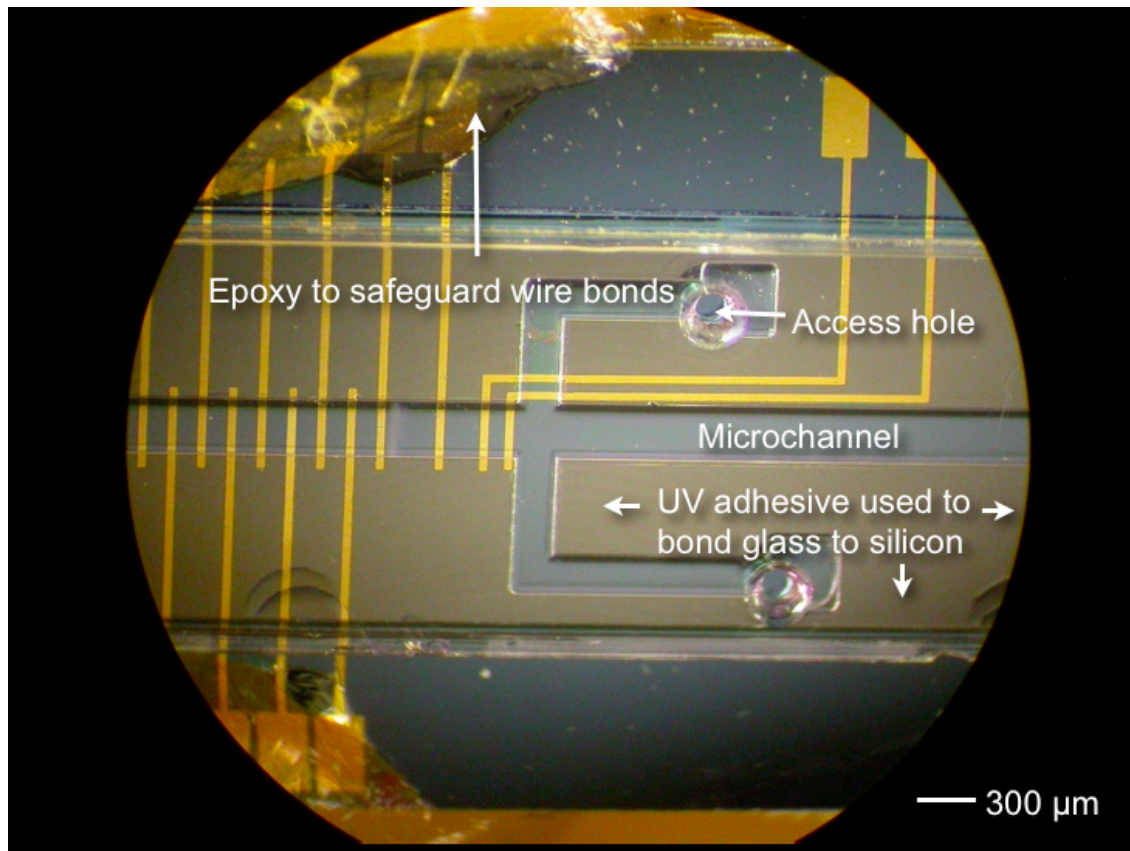


Figure 12. A microscopic image of the device showing the access holes for sample inlet and the epoxy used to safeguard the wire bonds.

#### **4.4 Microdevice Usage**

DNA samples were loaded into the microchannel and access holes were sealed with removable adhesive to prevent evaporation. The same device could be used repeatedly for multiple samples after thoroughly rinsing the microchannel with DI water. Comparison of results between new and re-used devices indicated that no appreciable electrode fouling (as evidenced through accumulation of fluorescent residue on the electrodes or glass channel walls, or through significant deviations in electrode capture response) occurred as a consequence of repeated use when these cleaning procedures were followed.

#### **4.5 Imaging and Detection**

The electrode capture process was imaged in two ways. Most experiments were performed using an Olympus SZX-12 fluorescence stereoscope and a CCD-300 cooled CCD camera (DAGE-MTI). For kinetic studies, an Axioskop-2 Plus microscope (Carl Zeiss) was used with an Orca-ER digital CCD camera (Hamamatsu) (Fig. 13). A combination of Openlab software (Improvision Inc) and customized MATLAB-based (The Mathworks) image analysis algorithms was used to acquire the intensity data and extract sample concentration from the fluorescence measurements. For flow visualization studies, a dilution of 1  $\mu\text{m}$  diameter carboxylate-modified polystyrene microspheres (FluoSpheres®, Invitrogen/Molecular Probes, Catalog # F-8823) were added to serve as tracers.





Figure 13. Experimental set-up showing the optical microscope with the attached CCD camera and stage control interfaced to the computer. Automations developed in-house using the Openlab software (Improvision Inc.) control the image capture and analysis in real time.

#### **4.6 The Electrode Array**

The electrode array is made up of rectangular shaped metal electrodes. Most of the devices designed have 50  $\mu\text{m}$  wide electrodes (Fig. 14). The effective length of the electrodes depends on the width of the glass channel used since that defines the electrode length lying with the channel and thus exposed to the sample. Initially both Gold and Platinum electrodes were used in the experiments. The results were identical and thus for further runs only Gold electrodes were used since they could be fabricated by thermal vapor deposition fabricated in-house.

The logic behind using an array of electrodes instead of a couple of electrodes was that this would enable higher electric fields at lower voltages resulting in faster capture of DNA and higher degree of focusing. The close spacing of the electrodes (225  $\mu\text{m}$ ) in the microchannel leads to electric fields of the order of  $\sim 40$  V/cm generated with minimal applied voltages ( $\sim 1$  V). The low voltages applied lead to the possibility to use the technique in battery operated devices for portable diagnostics applications.

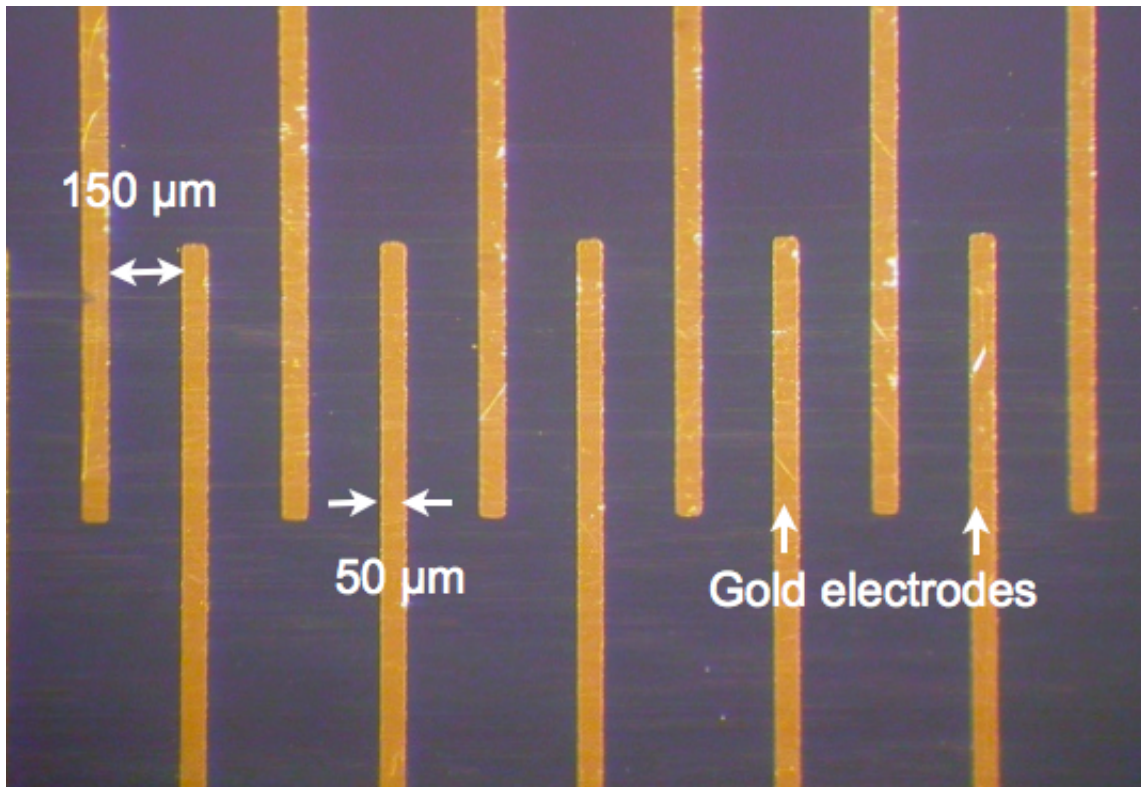


Figure 14. The electrode array as seen under a microscope. The electrodes are made up of a 1000 Å thick layer of gold deposited on 500 Å of chromium on a silicon substrate.



## CHAPTER V

### FINITE ELEMENT ANALYSIS SIMULATION

The capture release process was modeled using a finite element method model developed and solved using the software package FEMLAB 3.1 (COMSOL Inc.).

#### **5.1 Introduction**

A straightforward electrokinetic model was formulated using a system of differential equations expressing (i) conservation of total species flux due to diffusion and electromigration and (ii) conservation of charge, coupled through the electric field profile. The model was solved in 2-D using the finite element method subject to zero species flux and electrically insulating boundary conditions on all surfaces except the two electrodes, where a 1 V potential difference was imposed. Characteristic electrochemical data for DNA and ionic species comprising the TBE buffer were obtained from literature. A pair of adjustable parameters determined from fits to experimental data are used to introduce the observed dependence of the kinetic time constant on buffer concentration and addition of BME. Despite the relative simplicity of this model, it is capable of capturing the qualitative features of DNA migration toward the anode as well as the quantitative kinetics of enrichment expressed in terms of a first order exponential time constant. These results further substantiate the dominant role of electrophoretic transport in the electrode capture process.

Finally, we note that dielectrophoretic effects (which can be important in interdigitated electrode array configurations) are also expected to exert a relatively small influence under these conditions. This is because the DC electric fields employed here are of comparatively low magnitude and not strongly divergent, except perhaps in the immediate vicinity of the electrode corners. The electrodes used here, however, are much thicker (~150 nm) than those typically employed for dielectrophoretic trapping of DNA (~1-10 nm (23, 24)) where the objective is to maximize electric field nonuniformity at the corners.

## **5.2 Model Development and Results**

The single electrode capture process was modeled using the finite element method (FEM) with the software package FEMLAB 3.1 (COMSOL Inc.). A simplified theoretical framework was constructed subject to the following approximations: (1) electric field is unaffected by the charge on the DNA and its movement in solution, (2) reaction and generation of chemical entities are negligible, (3) electroosmosis (if present) can be represented by an equivalent current flux in the direction of the electroosmotic flow, and (4) conductivity, charge, temperature and mobility values remain constant. The fundamental physics associated with ionic species transport can then be modeled by coupling the electrokinetic flow to the electric field generated in the microchannel as follows:

1. Electrokinetic flow: The time derivative of the species concentration is related to the divergence of the total species flux due to diffusion and electro-migration. The migration term is proportional to the charge, mobility and electric field intensity at that location and the diffusive flux depends on the diffusion coefficient and the concentration gradient.

$$\frac{\partial c_i}{\partial t} + \nabla \cdot (-D_i \nabla c_i - z_i \mu_i F c_i \nabla V) = 0 \quad (2)$$

Here,  $c_i$  = ionic species concentration, mol/m<sup>3</sup>,  $D_i$  = diffusivity, m<sup>2</sup>/s,  $z_i$  = ionic charge, C/mol,  $\mu_i$  = ion mobility, m<sup>2</sup>/V·s,  $F$  = Faraday constant = 96,487 C/mol, and  $V$  = potential, V.

2. Electric field: The conservation law (Eq. 2) is then coupled to the electric field profile, where the electric field is represented as a gradient of the potential function.

$$E = -\nabla V \quad (3)$$

The current density in the conductive media can be expressed as:

$$J = \sigma E + J^e \quad (4)$$

Here,  $J$  = current density,  $\sigma$  = conductivity, and  $J^e$  = externally generated current density.

The static form of this equation of continuity, along with Eq. 2 gives:

$$\nabla \cdot J = -\nabla \cdot (\sigma \nabla V - J^e) = 0 \quad (5)$$

The domain geometry is defined to represent a 2-D side-view profile of a pair of capture-release electrodes. In this view, the electrodes are located on the bottom edge (i.e. at the floor) of the rectangular section of the microchannel (Fig. 15), with the DNA suspended in buffer in the above enclosed channel above it. Zero species flux and

electrically insulating boundary conditions are applied at all surfaces except the two electrodes, where a 1 V potential difference is imposed. Species mobilities are expressed as  $\mu_i = D_i/RT$ . The relatively high characteristic values of DNA mobility, however, introduce convergence problems because fluxes become dominated by migration (convective flux). This is dealt with by introducing an artificial diffusion component (streamline, Petrov-Galerkin: compensated, tuning parameter = 0.5) to stabilize the solution. Characteristic electrochemical data are obtained from literature (Table 2).

Table 2. Characteristic species parameter values used in the simulation studies (40-42).

<b>Sample Component</b>	<b>Mobility (m<sup>2</sup>/V s)</b>	<b>Diffusivity (m<sup>2</sup>/s)</b>	<b>Concentration (g/L)</b>
Tris	3.00 x 10 <sup>-13</sup>	8.00 x 10 <sup>-10</sup>	15.75
Borate	4.00 x 10 <sup>-14</sup>	1.00 x 10 <sup>-10</sup>	2.78
DNA	1.55 x 10 <sup>-13</sup>	5.00 x 10 <sup>-12</sup>	0.012

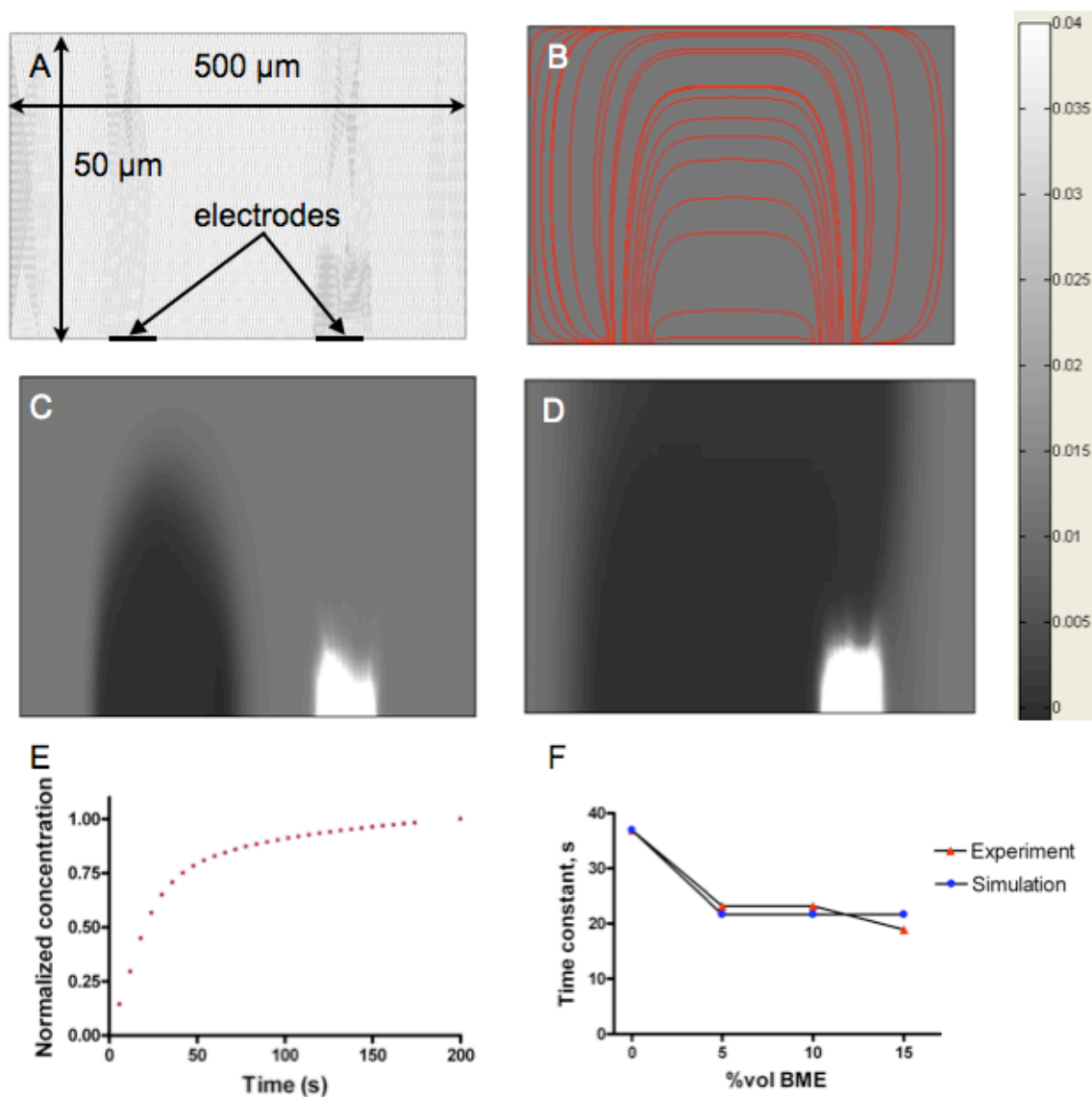


Figure 15. Electrode capture process simulated for DNA initially at 12  $\mu\text{g/ml}$  in 1x TBE buffer under a 1 V applied potential. (A) shows the mesh generated within the geometry, and (B) shows the electric field lines in the geometry. Simulation results depicting the migration and capture of DNA after elapsed times of (C) 10, and (D) 200 s. The grayscale calibration on the right denotes the concentration from 0 to 0.04 g/ml. Concentrations higher than 0.04 g/ml that are generated on the anode appear white (C,D) on the simulation snapshots. (E) Simulated transient enrichment in DNA concentration at the anode. (F) Comparison of simulated capture time constants with corresponding experimental results (parameter values of  $f_1 = 0.168$  and  $f_2 = 2.3$  were used here).

Despite its relative simplicity, this model is capable of capturing many features of the electrode compaction process (Fig. 15). As a potential is applied, the DNA migrates toward the anode following the field lines that are established between electrodes. The enrichment in DNA concentration at the anode agrees with corresponding observations of increased fluorescence intensity, and can be quantified to obtain kinetic parameters as is done experimentally. Quantitative kinetic predictions, however, require consideration of the interplay between the parameters in Table 2. From the experimentally obtained values of the time constant, we notice that the kinetics are accelerated (higher time constants) at lower TBE concentrations (up to 1x). The addition of BME, further accelerates the capture. In case of TBE, the mobility of DNA exhibits a dependence on buffer concentration (43). In order to incorporate this behavior into the model, we define an effective mobility for the DNA with in terms of two adjustable parameters,  $f_1$  and  $f_2$ ; where  $f_1$  accounts for the change in mobility with TBE concentration and  $f_2$  for the change observed with addition of BME ( $\mu_{eff} = \mu \cdot f_1 \cdot f_2$ ). The values of the parameters are determined from experimental data, yielding  $f_1 = 0.073x^2 - 0.371x + 0.466$  and  $f_2 = -7.7848x^2 + 32.892x - 22.812$ , where  $x =$  TBE concentration (viz. 1, 2, 3 for 1x, 2x, 3x buffers respectively). The ability of this relatively simple model to capture the essential features (both qualitatively and quantitatively) associated with the electrode capture process provides further evidence that electrophoretic transport of DNA is the dominant process.

## CHAPTER VI

### LABEL-FREE DETECTION OF CHARGED BIOMOLECULES

#### 6.1 On-Chip Detection Strategies in Literature

A number of different approaches have been investigated to perform biomolecule detection in microfluidic systems (44). Optics-based technologies (e.g., laser induced fluorescence (LIF)) are among the most mature and popular methods. In LIF, fluorophores with specific spectral response characteristics are conjugated to DNA or other biomolecules of interest in order to generate detectable fluorescence signals. The drawbacks of these types of techniques are that they require additional time and expense to perform chemical labeling, and the fluorescent tags may render the biomolecules incompatible with subsequent reactions. A more important drawback of LIF is that sensitive macro-scale optical detection instrumentation is typically needed because the levels of emitted fluorescence are inherently low. The size, complexity, and cost of these components can often negate most of the benefits of miniaturization.

Electrochemical detection methods have also been widely explored as label-free alternatives to optics-based approaches because they are capable of providing direct electrical output signals and are highly amenable to miniaturization. Electrochemical approaches based on amperometry, potentiometry, and conductimetry have been demonstrated for detection of analytes during capillary electrophoresis (45) as well as for sensing of hybridization at functionalized electrode surfaces (46). Although these methods are generally robust for detecting charged molecular species, detection of DNA

in free solution requires addition of electrochemically active intercalation agents and is not particularly sensitive to low DNA concentrations (47, 48). Detection methods based on mass spectrometry (MS) also show great promise (49), but a variety of engineering challenges remain to be overcome before all the associated instrumentation can be fully miniaturized and integrated with other microfluidic components. Finally, surface plasmon resonance (SPR) techniques are also becoming more widely used for detection of binding events at surfaces, but cannot generally be applied for analysis of species in free solution or unbound species near the surfaces.

The ability to quantitatively detect label-free charged biomolecules like DNA and proteins in free solution would introduce new opportunities to greatly simplify the physical and operational design of integrated lab-on-a-chip devices. This capability also has the potential to enable the progress of on-chip processes to be observed and regulated in real-time.

## **6.2 Experimental Observations of Label-Free DNA Detection on the Capture Electrode**

It was observed that when the same dsDNA samples used in the capture-release experiments were used without any fluorescent labeling (eg. YOYO-1), the compacted DNA on the anode, was scattering incident white light intensely (Figs. 16 and 17).



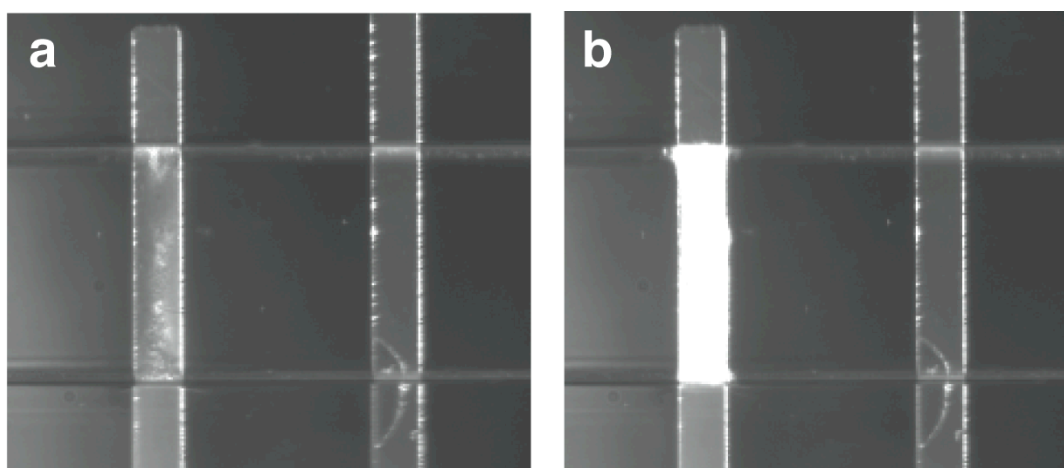


Figure 16. DNA visible under white light (100 bp DNA ladder in 1X TBE buffer). (a) No voltage applied to electrodes. (b). Reflected band is evident at the anode after applying a 1.5 V potential between electrodes for ~1 min.

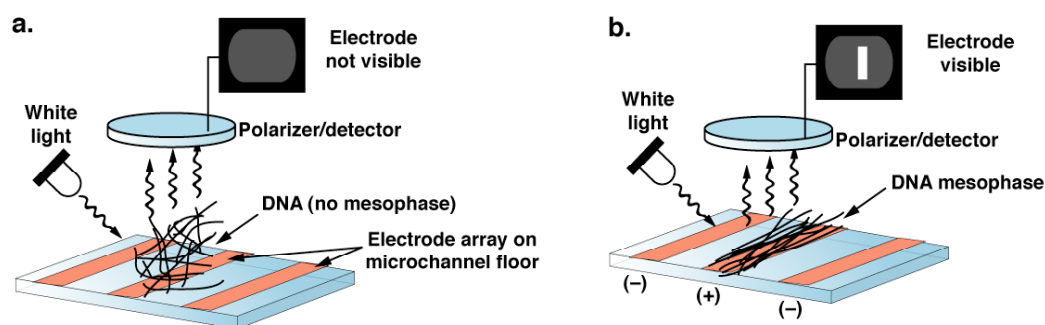


Figure 17. Schematic illustration of experimental observations of label-free DNA detection in free solution. (a) Initially, DNA in solution inside the microchannel is isotropically oriented. (b) When the DNA is compacted to an ultra-high concentration at the anode surface by applying a 1–2 V potential between electrodes in the array, a concentrated DNA plug is formed at the anode and appears intensely visible under white light. Drawings are not to scale.

The light scattering phase that is visible in this experiment, if observed using transparent glass devices instead of silicon devices, reveals a multicolored phase (Fig.

18). The colors were visible in both white light and polarized light microscopy. This provides evidence of light diffracting nature of the phase.

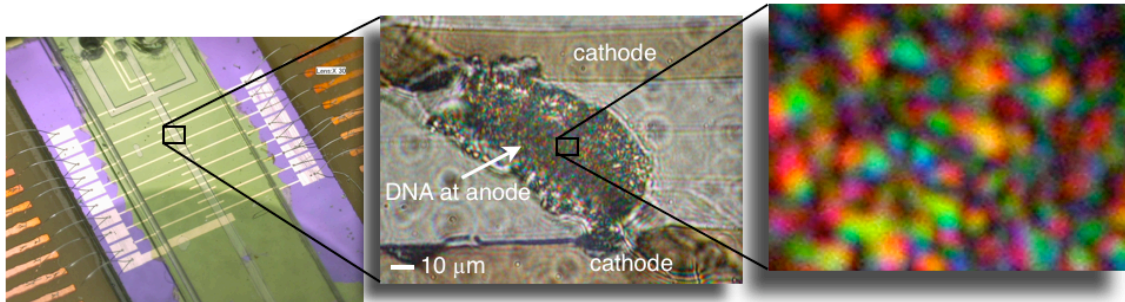


Figure 18. The lab-chip on the left shows the addressable electrode array along the microchannel floor. Zooming into the microchannel reveals the DNA mesophase visible under polarized white light which forms on application of an electric field, and reveals brilliant colors under 400X magnification on the far right. The magnified images are of a glass device and not a silicon device as shown on the left.

On removal of the applied electric potential, the phase quickly ( $\sim 5$ - $10$  s timescale) dissipates back into the buffer.

### 6.3 Fundamental Characterization of the Optical Phenomenon

There are a number of possible effects that could describe the results that are observed in the aforementioned experiments. Some of the likely causes are:

- Mesophase (liquid crystal phase) formation
- Scattering and diffraction of light
- Refractive index change

A series of experiments were undertaken and a number of new devices were fabricated to characterize the phase forming on the electrode surface.

### **6.3.1 Mesophase Formation**

Mesophase formation is possible because the closely spaced electrodes within the array ( $\sim 200 \mu\text{m}$ ) enable electric fields to be generated that are strong enough to confine the DNA at the surface of the anode (50–100 V/cm) by applying very low potentials ( $\sim 1\text{--}2 \text{ V}$ ). In this way, the DNA experiences two-dimensional focusing (Fig. 19) and compaction into an ultra-concentrated layer that is only a few microns thick ( $<5\mu\text{m}$  from finite simulation results in chapter V, Fig. 15). The high degree of confinement in this zone can become sufficient to promote formation of a mesophase owing to a combination of high concentration and excluded volume interactions that imparts a change in optical properties such that the collected biomolecules can become clearly visible under white light.

### **6.3.2 Experimentation and Results**

The single electrode capture process has been modeled in chapter V using a simplified 2-D finite element approach with the software package FEMLAB 3.1 (Fig. 15, chapter V). As a potential is applied, the DNA migrates toward the anode following the field lines that are established between electrodes. The enrichment in DNA concentration at the anode agrees with our observations of increased fluorescence intensity, and can be quantified to obtain kinetic parameters that are also in agreement

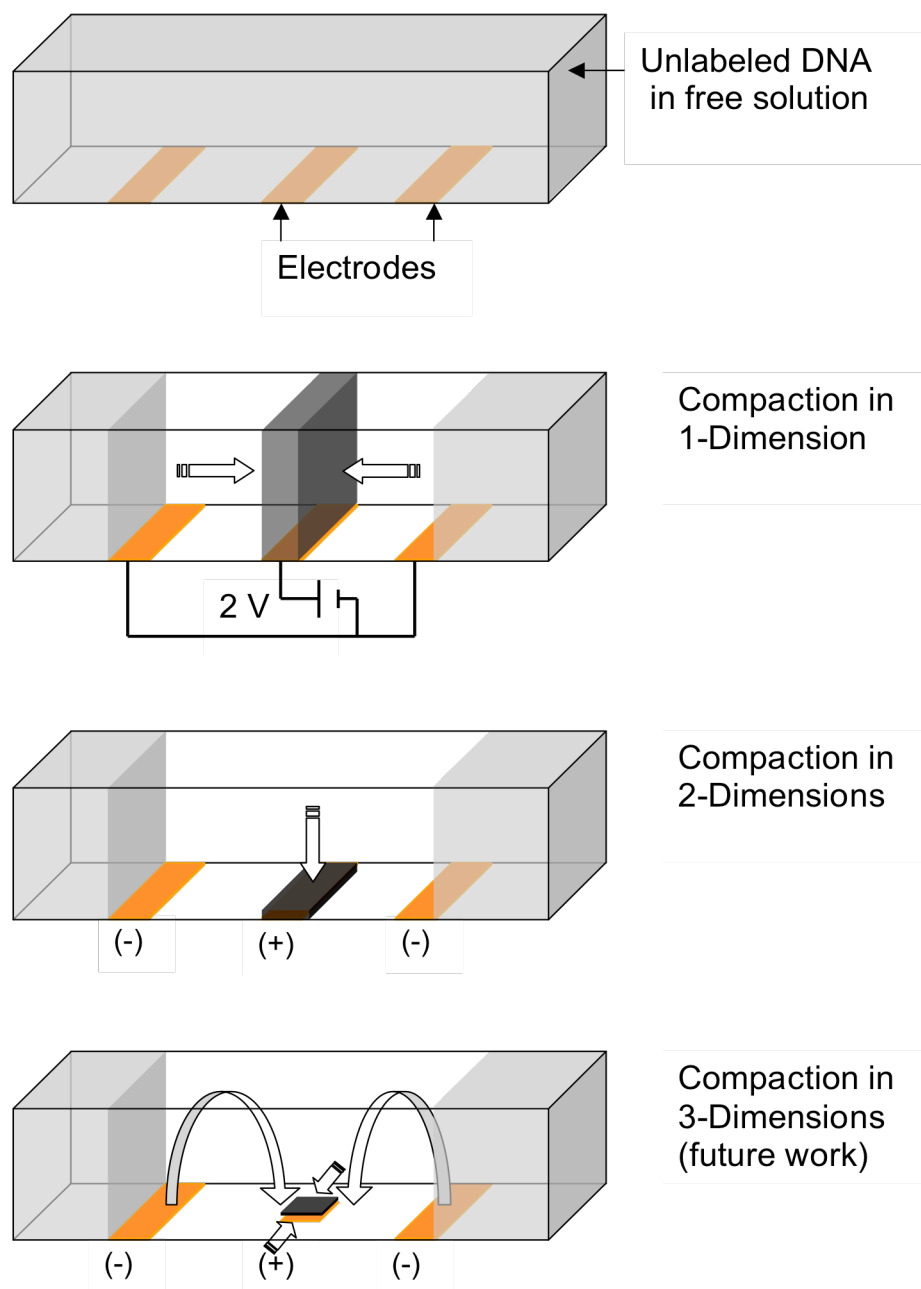


Figure 19. A schematic of the compaction of DNA occurring during the dual-focus.

with experimental measurements (chapter V). A key observation is that the captured DNA is simultaneously concentrated in both the axial and vertical planes, resulting in confinement within a very thin layer ( $< 5 \mu\text{m}$ ) at the electrode surface (Fig.15). This high degree of compaction introduces the possibility of inducing a transition to an ordered mesophase due to excluded volume interactions.

In order to illustrate this phenomenon a series of preliminary experiments were undertaken whose key results are summarized in Fig. 20. First, the overall device design consists of a silicon or glass device that incorporates an array of microfabricated gold electrodes ( $50 \mu\text{m}$  wide,  $225 \mu\text{m}$  spacing). In the glass substrates, a very thin gold layer ( $15 \text{ nm}$ ) was deposited so that it could remain optically transparent and enable the mesophase to be viewed under transmitted illumination through crossed polarizers. As seen before, an etched glass microchannel is bonded to the electrode array device using UV glue to create an enclosed fluidic channel with electrodes positioned along the floor, and wire bonded to a PC board to establish electrical contact with the array (Fig. 11). Experiments involve injecting DNA into the microchannel (100-bp ladders suspended in supplied, 1x Tris-Borate EDTA, and histidine (50 mM) buffers were used as test samples) and sealing the loading ports to prevent evaporation. The device is then placed under a microscope and the compaction process is initiated by applying a 1–2 V DC potential.

### Device Assembly And Experimental Set-Up

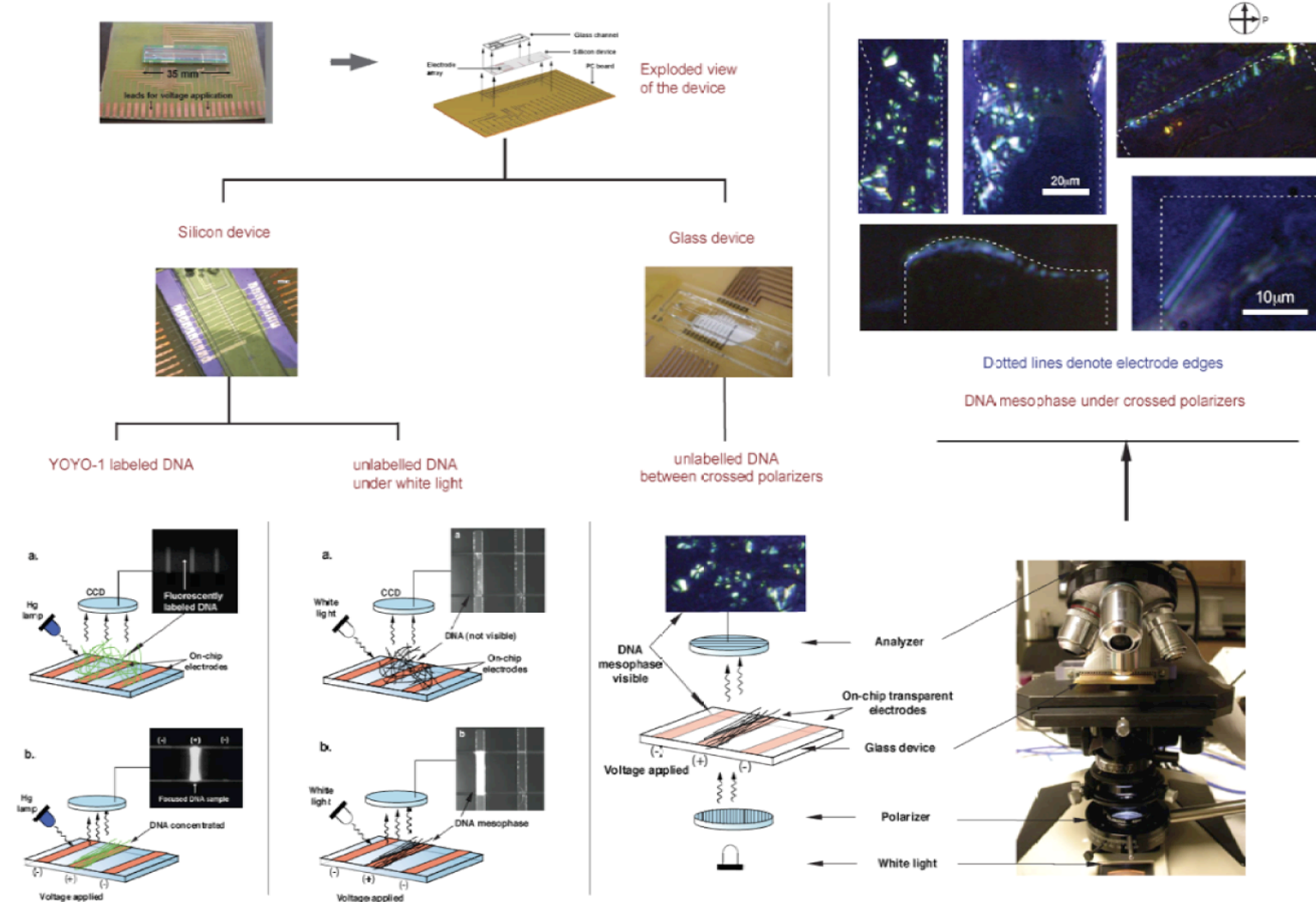


Figure 20. Overview of the experimental setup used to investigate mesophase formation during the electrode capture process. Experiments were performed under both reflected illumination and by observing transmitted light through crossed polarizers using optically transparent electrodes.

In order to determine whether this effect could be a manifestation of the formation of an ordered mesophase arising due to the high level of concentration enhancement at the electrode surface, the experiments were repeated using devices with optically transparent electrode arrays fabricated using indium tin oxide (ITO) or by deposition of a very thin layer of gold (results using gold electrodes are shown in Fig. 20). Here, distinct birefringent textures become evident when the capture anode is viewed through crossed polarizers (Fig. 20, right). These textures nucleate along the edges of the electrodes, eventually extending more broadly over the electrode surface with an appearance characterized by distinct highly birefringent domains. The edges of the electrodes in Fig. 20 (denoted by dashed white lines) appear irregularly shaped as a consequence of electrochemical dissolution at potentials above  $\sim 1.5$  V. The timescale of this dissolution is slower than the capture process (and we observe identical compaction kinetics as with thicker electrodes). Mesophase formation is completely reversible, quickly dissipating when the potential is switched off.

### 6.3.3 Device Design

The use of transparent electrodes is essential for these studies because it allows us to view the capture process under transmitted light through crossed polarizers. Two ways were explored to construct transparent electrodes in this work. First, electrodes constructed from indium tin oxide (ITO) in microfabricated electrode arrays purchased from ABTECH Scientific were used. Unfortunately, the capture performance was not as robust as in the metal electrode devices, possibly due to unexpected electrochemical reactions occurring at the ITO surfaces. There was greater success using microelectrode arrays fabricated by depositing ultra thin films of gold ( $\approx 15$  nm) that are both electrically conductive and optically transparent. As shown in Fig. 20, these electrodes have led to clearly observe birefringence within the expected mesophase, although some electrochemical erosion also occurs at the electrode edges. However, these results were obtained without optimizing fabrication process parameters to maximize stability. In addition, the spacing between electrodes can be reduced (and more electrodes can be added to the array) in order to drastically reduce the voltage levels that need to be applied to generate the required electric fields. A reduction in inter-electrode spacing by a factor of only 2 – 4 would reduce the necessary potentials to well below 1 V. Since erosion problems were only observed above 1.5 V, this strategy will greatly reduce (and perhaps eliminate) these electrode dissolution issues while still maintaining an optically transparent design. A wider range of process parameters (metal film thickness, annealing, etc.) can be explored to further optimize performance.



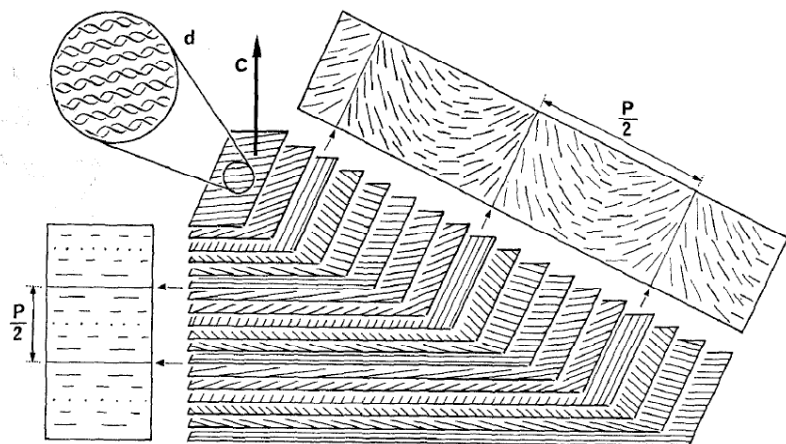


Figure 21. Schematic illustration of cholesteric organization in double-stranded DNA. The structure is characterized by layers of oriented DNA molecules that are rotated with respect to neighboring layers with pitch  $P$  (diagram is reproduced from (51)).

The development of distinct birefringent textures at the electrode surface provides evidence for the formation of an ordered mesophase. The ability of DNA to form liquid crystal mesophases has been widely observed (52, 53), dating back to the seminal observations of Robinson in 1961 (54). In addition to being of interest from a physical standpoint, the capacity to self assemble appears to play an important biological role in-vivo where the process is mediated via the activity of ionic condensation agents that enable DNA to be more compactly packaged (55-57). In-vitro studies have shown that DNA undergoes a transition from an isotropic state to cholesteric ordering at concentrations in the vicinity of 160 mg/mL (Fig. 21). This is followed by a transition to 2-D hexagonal ordering at  $\sim 380$  mg/mL, and to a 3-D hexagonal structure at  $\sim 670$  mg/mL. These are approximate values, as the actual transition concentrations depend on

the DNA fragment length and the ionic strength of the surrounding buffer medium (58, 59). These liquid crystalline phases are challenging to study because it is difficult to produce DNA solutions at the extremely high levels of concentration that are required (52). One method of sample preparation involves the re-suspension of lyophilized DNA sample in a small amount of buffer to obtain the desired concentration. Another method involves the introduction of a polymeric condensation agent like poly(ethylene glycol) to nucleate phase separation. In both cases, the final concentration is very sensitive to evaporation and complete dissolution of the DNA can be difficult to achieve.

#### 6.3.4 Calculation of Critical Concentration of Mesophase Formation

In order to estimate whether sufficiently high concentrations could be achieved in the compaction zone near the anode to drive the transition to an ordered mesophase, we follow Semenov-Khokhlov theory for semi-flexible polymers where the critical volume fraction  $f$  required to form a fully nematic liquid crystalline phase scales as  $f = 5.7 d/L_p$ , where  $d$  is the diameter of the molecule and  $L_p$  is its persistence length (60, 61). For double-stranded DNA ( $d \sim 2$  nm,  $L_p \sim 50$  nm), this corresponds to a value of about  $f = 0.22$ . Now, as an example we consider the case of a sample composed of 500 bp double-stranded DNA fragments. We can calculate the mass of a single DNA molecule,  $m_{DNA}$ , (taking the molecular weight of one base pair as 660 Da), and estimate its volume,  $V_{DNA}$ , by modeling it as a cylinder of length = 500 bp \* 0.43 nm/bp and diameter = 2 nm (62). This allows us to determine the DNA concentration that corresponds to  $f = 0.228$  from  $c_{f=0.228} = 0.228 * m_{DNA} / V_{DNA} \approx 180$  mg/mL. *This value agrees with the  $\sim 160$  mg/mL*

*threshold concentration reported for the isotropic to cholesteric phase transition (63).* Since the DNA sample in these experiments is initially at a concentration of 12  $\mu\text{g/mL}$ , this suggests that the level of compaction achieved is *at least*  $180 \text{ mg/mL} \div 12 \mu\text{g/mL} = 15,000\text{X}$  at the electrode surface. These scaling arguments combined with the experimental observations support the hypothesis that the electrode compaction process is capable of inducing a transition to an ordered mesophase.

### 6.3.5 Refractive Index Change

The refractive index of the phase that is visible is bound to be different than the surrounding buffer since it is made up of a dense phase of DNA molecules compacted in a small volume. The dependence of the refractive index of a medium on its optical density is given by:  $\eta = 1 + k(\lambda) \cdot \rho$ , where  $\eta$  = the refractive index of the medium,  $k(\lambda)$  = wavelength dependant parameter, and  $\rho$  = optical density of the medium.

The change in the refractive index at the concentrated phase, can lead to interference between the reflected or scattered light rays from the surface of the phase and the reflected light rays from the surface of the capture electrode (Fig 22). A common manifestation of this is the Schlieren effect that can give a similar optical appearance as is observed on top of the capture electrodes under white light illumination. Preliminary experiments to test the presence of this effect with diode-lasers were inconclusive. It is thus suggested to carry out further investigations using more reliable laser sources in order to quantify this effect.

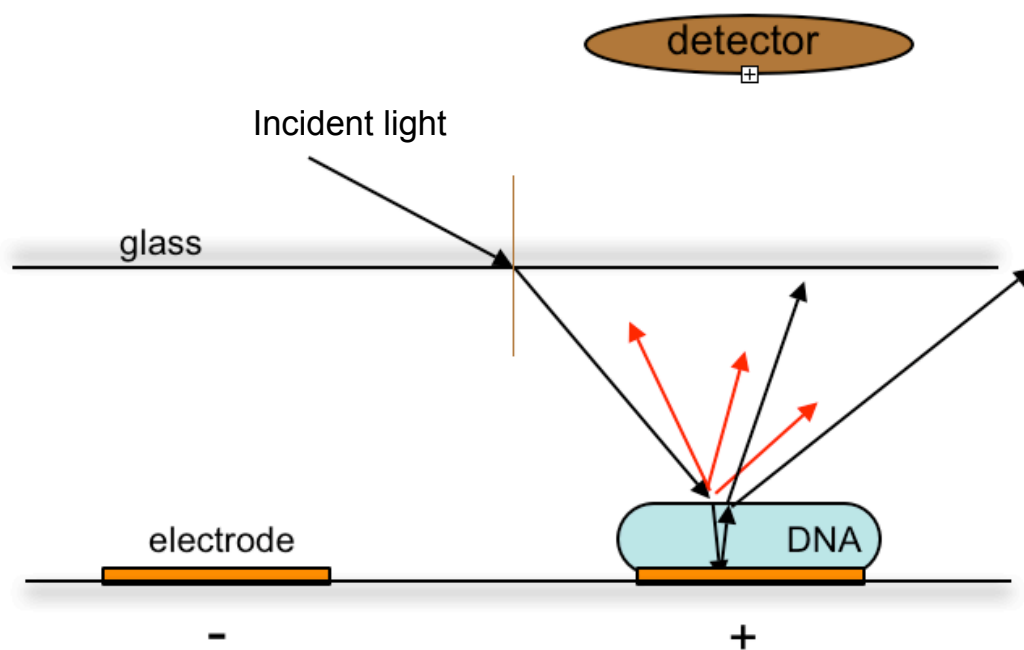


Figure 22. Schematic representation of the effect of incident light scattering and refractive index changes occurring at the surface of the capture electrode.

Another possibility that was looked at was stabilization of bubble nuclei by the concentrated DNA phase. DNA has surfactant properties and being at a high concentration at the electrode surface where electrolysis occurs, could lead to stabilization of the gas bubbles as soon as they start forming, so they do not coalesce easily. A large number of these tiny bubbles would potentially be able to scatter incident white light and give the observed experimental results. In order to test this hypothesis, Tween 20 and Tween 80 (detergent species) were added in 1X TBE instead of dsDNA. The capture was carried out and there was no scattering observed as in the case of DNA. This was tested for a range of concentrations ( $5\mu\text{g/ml}$ - $100\mu\text{g/ml}$ ) of Tween 20 and Tween 80 prepared in 1X TBE and Histidine. None of these experiments revealed any

light scattering at the capture electrode. Inferring from the results, it seems unlikely that the optical phenomena observed is due to scattering from bubble nuclei stabilized by DNA. A more definitive answer about the specificity of the effect can be arrived at by performing the capture with chemical species that have a similar structure to DNA but not the long semi-rigid rod structure. This would answer whether the semi-rigid rod structure is necessary for the effect to occur. Heptakis(6-Osulfo)- $\beta$ -cyclodextrin and Heptakis(2-Omethyl-3,6-di-O-sulfo)- $\beta$ -cyclodextrin are two appropriate candidates for this experiment. They are composed of seven sugar molecules forming a ring shape. The top view thus looks structurally similar to a DNA molecule, and these molecules are charged just like the DNA phosphate backbone. The major difference is that these molecules are much much smaller than the 100bp ladder employed in the capture experiments. Results from these runs would answer whether the optical effect is specific to large biomolecules like DNA and proteins that are capable of forming ordered structures at high concentrations.

### **6.3.6 Directions for Further Characterization**

The intense scattered light could be a result of a few optical effects working independently. The highly concentrated DNA at the surface of the electrode will increase the optical density and consequently, the refractive index of the region on top of the electrode to bend the incident light closer to the normal. This could very well be augmenting the light intensity observed on top of the electrode. In addition, the conditions under which the phase is observed are similar to the experiments done to

measure Surface Enhanced Raman Scattering (SERS) as SERS is active at visible wavelengths of light for gold electrodes with molecules in close proximity of the gold electrode. An experiment with a monochromatic light source instead of a white light source, such as a laser would reveal answers to these possibilities. In addition, observation of a Raman shift, if any, would confirm the presence of the SERS.

Newer designs can incorporate electrode arrays with spacings and shapes that tailor the electric field topology. Anodes have been designed that are much smaller ( $\sim 10\mu\text{m}$ ) than the current size (e.g., pads or “islands”) in order to enable even higher levels of compaction to be achieved at the electrode surface. Deposition of polyimide thin films over the electrodes, that can be further patterned (e.g., by buffing) to induce a preferred surface alignment state, has been investigated. This has not worked well yet due to problems encountered during in-house fabrication. The influence of condensation agents that either enhance or retard mesophase formation can also be explored.

This phenomenon needs to be studied in greater detail so that the fundamental processes that underlie formation of this mesophase can be understood to a greater extent. This will help to control and optimize the process so that new bioanalysis devices that make use of this effect can be rationally designed.

#### **6.4 Label-free Protein (Lysozyme) Detection**

An important application is to extend our DNA-based studies to proteins using egg white lysozyme as a model system. Proteins are charged biomolecules like DNA,

but differ in several key details including (1) a charge to size ratio that can vary depending on the amino acid sequence, (2) a molecular structure that is more flexible (characteristic persistence lengths of a few nm, as compared to  $\sim 50$  nm for double-stranded DNA), and (3) the ability to assume complex folded structural topologies by hydrogen bonding. Thus, although the general electrophoretically driven compaction process is applicable to proteins, the nature of the concentrated layer formed at the electrode surface may not be identical to DNA. In order to demonstrate proof of concept, experiments using egg white lysozyme (Sigma-Aldrich) were carried out. Using a 4% w/v initial concentration in 1x TBE buffer, lysozyme sample was collected at an electrode with sufficient enrichment to make it visible under white light illumination with no modification to the device design (Fig. 23). The sample became visible in 10 – 20 s after applying the voltage, and dissipated 5 – 10 s after the voltage was switched off.

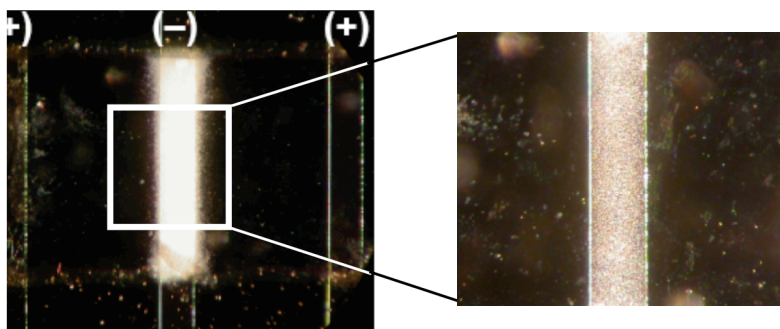


Figure 23. Proof of concept for label-free protein detection. Egg white lysozyme protein (4% w/v in 1x TBE buffer) is concentrated at an electrode surface ( $50 \mu\text{m}$  wide) by performing a dual focus with  $\sim 2.5$  V potential. The compacted protein becomes concentrated enough to be visible under white light illumination in 10–20 s.

The capture process can be tuned by adjusting the buffer pH relative to the protein's isoelectric point (e.g., to localize the sample at either the anode or the cathode). It is required to quantify these effects by systematically studying compaction efficiency over a range of buffering conditions in order to determine optimal parameters to maximize capture speed and detection sensitivity (e.g., number of molecules collected per electrode pair). Another issue involves determining the nature of the protein molecular structure in the compacted layer. Although proteins are semi-flexible, they are generally less rigid than double-stranded DNA thereby raising the threshold concentration for transition to an ordered mesophase. However it is also possible that the protein concentration at the electrode surface may become high enough to locally alter the refractive index thereby creating a zone within which there is an abrupt index change resulting in enhanced reflectivity upon compaction. This can be tested by quantifying the thickness of the compacted layer using the confocal microscopy and using the local protein concentration to estimate the corresponding refractive index change. The change in compaction efficiency can be studied with addition of denaturants (e.g., formamide,  $\beta$ -mercaptoethanol) that may alter the molecular configuration and promote a different compaction density. Finally, the design of electrode shapes incorporating curvature or angles that will generate locally high electric fields specifically favorable for compaction under ionic conditions relevant to proteins can be explored. These designs can be guided by finite element simulations to predict the topology of the electric field lines associated with each geometry. Modifications to the electrode size can also be explored to achieve enhanced multidimensional compaction (Fig. 19).



## CHAPTER VII

### ADVANCED APPLICATIONS

In section 2.4 the *dual focus* scheme is discussed whereby the negative electric potential is applied to electrodes on both sides of the capture electrode. This leads to sandwiching the DNA on top of the capture electrode that lies in the middle (that is at a higher electric potential). The dual focus can enable additional functionality with the electrode array. Some of these applications and possibilities are described below.

#### 7.1 Buffer Exchange

A key consideration in performing sequential DNA analysis operations in microfluidic systems is the requirement that many of these processes take place in specific buffer environments. This is an issue, for example, in the case where an electrode capture process is used to concentrate products from an on-chip biochemical reaction prior to gel electrophoresis because mismatches in conductivity between the sample and running buffers can degrade separation performance. These issues can be straightforwardly addressed by combining the electrode capture system with a superimposed bulk hydrodynamic flow (Fig. 24). If the strength of the flow is selected such that hydrodynamic force (Fig. 25) does not exceed the electrostatic forces confining the captured DNA at the anode, a different buffer solution can be introduced into the microchannel so that the DNA will be re-suspended in a new environment upon release.

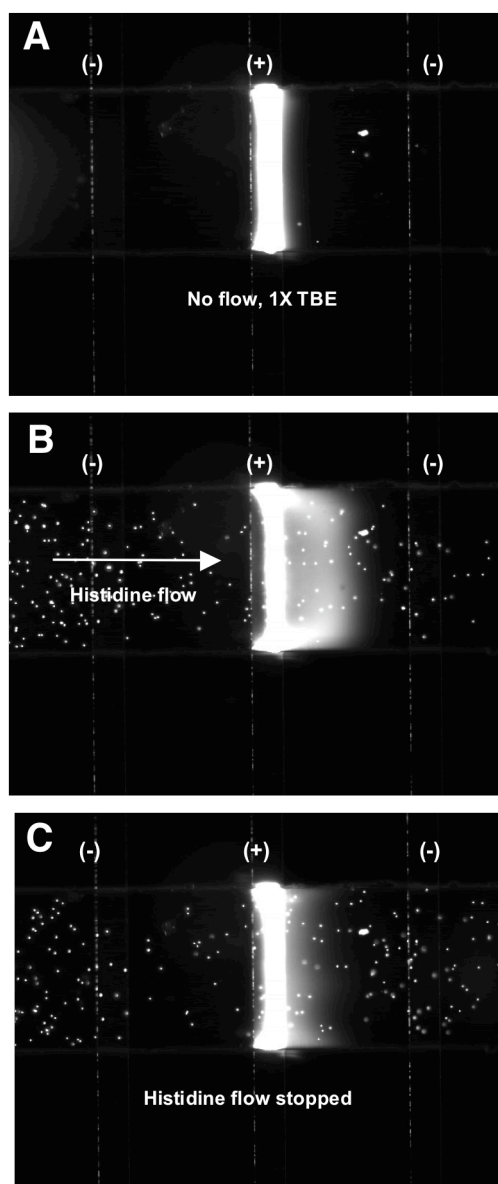


Figure 24. Buffer exchange. (A) A DNA sample initially at  $12 \mu\text{g/ml}$  in  $1\times$  TBE buffer with 10% (vol/vol) BME is captured at the central anode by dual focusing. (B) A hydrodynamic flow is introduced by placing a drop of 50 mM histidine (no BME added) labeled with carboxylated polystyrene microsphere tracers at the microchannel inlet, generating velocities ranging from  $11$  to  $18 \mu\text{m/s}$  (flow direction is from left to right). Depending on the flow velocity, the captured DNA is partially swept downstream from the electrode surface but remains confined between cathodes (2.4-V potential). (C) Captured DNA returns to the anode when the flow stops. The sample can then be released and resuspended in the new buffer environment when the potential is switched off.

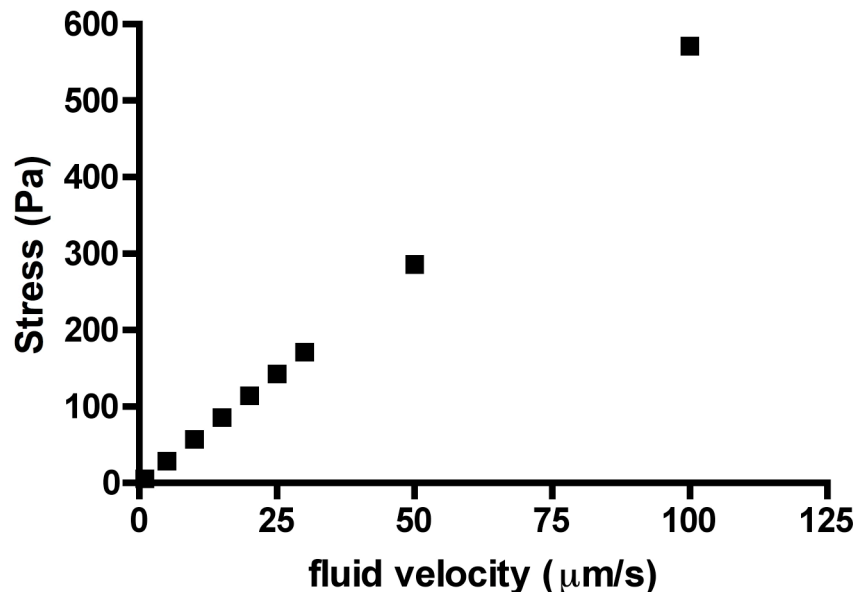


Figure 25. Stress acting on the surface of electrodes due to flow of buffer in the microchannel ( $50\mu\text{m} \times 300\mu\text{m}$  cross section channel).

## 7.2 Possibilities for Application of Capture-Release

The label-free detection work has demonstrated that a birefringent mesophase can be reversibly formed by applying low voltages across an electrode array inside a microchannel. This is a significant observation because:

- (1) it introduces new opportunities for DNA detection in microfluidic systems, and
- (2) it may allow us to create a new platform to enable observation and manipulation of DNA self assembly and packaging.

The extent to which the nanostructural ordering can be actively tuned in response to hybridization can be investigated. Confocal microscopy can be employed in these

studies. These binding events would be expected to disrupt local molecular alignment, frustrate ordering, and delay the mesophase transition thereby making hybridization detectable without the need for samples to be pre-labeled with conjugated fluorophores.

Since DNA appears to condense into a mesophase in the device, this technique can be used in gene transfection research where the major challenge is to condense and incorporate the engineered genetic DNA into the cell or nucleus of the target cell. The proximity to the electrode would provide electroporation (increased porosity of the cell wall by application of electric field).

With protein concentration occurring with ease on the electrode surface, the device can be used to test for protein crystallization studies and may especially help in speeding up the crystallization times especially of engineered proteins that can take days and even months to crystallize.

## CHAPTER VIII

### PORTABLE INTERFACE FOR LAB-ON-A-CHIP

Microfabricated devices generally need some laboratory equipment for interfacing with electrical power sources to drive the mechanisms designed on-chip and specialized light microscopy to detect and analyze the sample. Such considerations drag the disposable chip back into the lab environment for analysis purposes. In order to demonstrate the possibility of having a portable device that has an electrical interface to couple with lab-on-a-chips, a Field Programmable Gate Array (FPGA) was programmed to work as a portable handheld DNA concentration device using the capture-release electrode array used in this work.

#### **8.1 Field Programmable Gate Array (FPGA)**

A prototype portable analysis device is envisioned using the Nexys© platform (Digilent Inc.) that has an on-board Field Programmable Gate Array (FPGA) (Xilinx XC3S200) and leads for electrical connection to the bio-analysis chip in collaboration with the School of Computing and Engineering at University of Missouri, Kansas City (Fig 26). A FPGA is a semiconductor device that contains programmable logic components and programmable logic interconnects. The on-board memory is programmed through the USB (Universal Serial Bus) interface using a personal computer and programming language Verilog® to execute a series of electronic operations to achieve the objective whether it be on-chip DNA concentration through

capture-release or more complex future analysis protocols for lab-on-a-chip applications. It has 8 sliding switches and 4 push buttons on-board so that a number of tests could be programmed into the memory and user input can be done using these buttons, in case the device is powered by batteries, especially if a USB port is inaccessible in a particular scenario. The disposable analysis biochip can be simply slid into the 100-pin connector located at the edge of the Nexys platform board to generate the electrical contacts between the two.

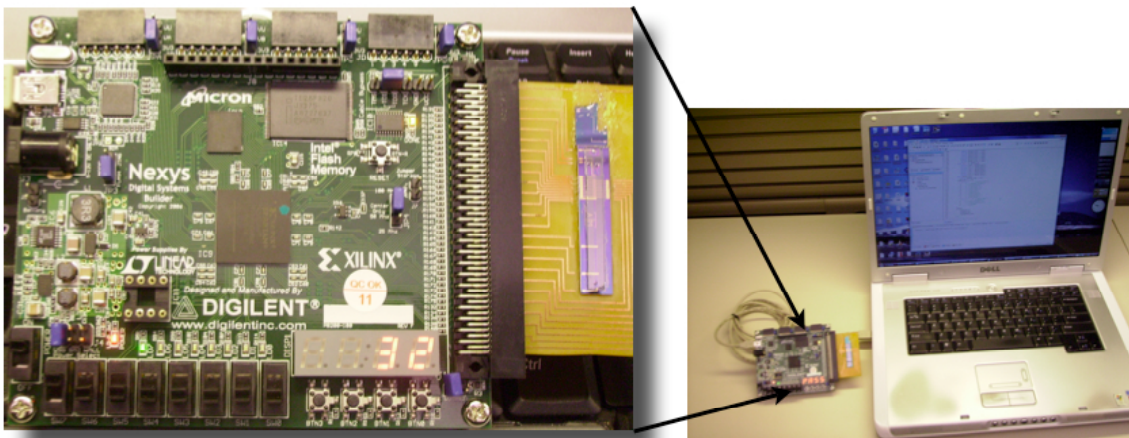


Figure 26. The capture-release chip is attached to an FPGA board that is connected and programmed through a USB cable using a personal computer.

USB is the most popular data interface for peripheral devices in personal computing. USB was originally developed for personal computers but has since been incorporated in handheld computers and smartphones. The handheld device can be programmed for stand-alone operation using AA batteries or alternately, it can utilize the

USB port itself as a power source (~3.3-5 V supply, 2.5 W maximum ) The block diagram of information flow is represented in Fig. 27.

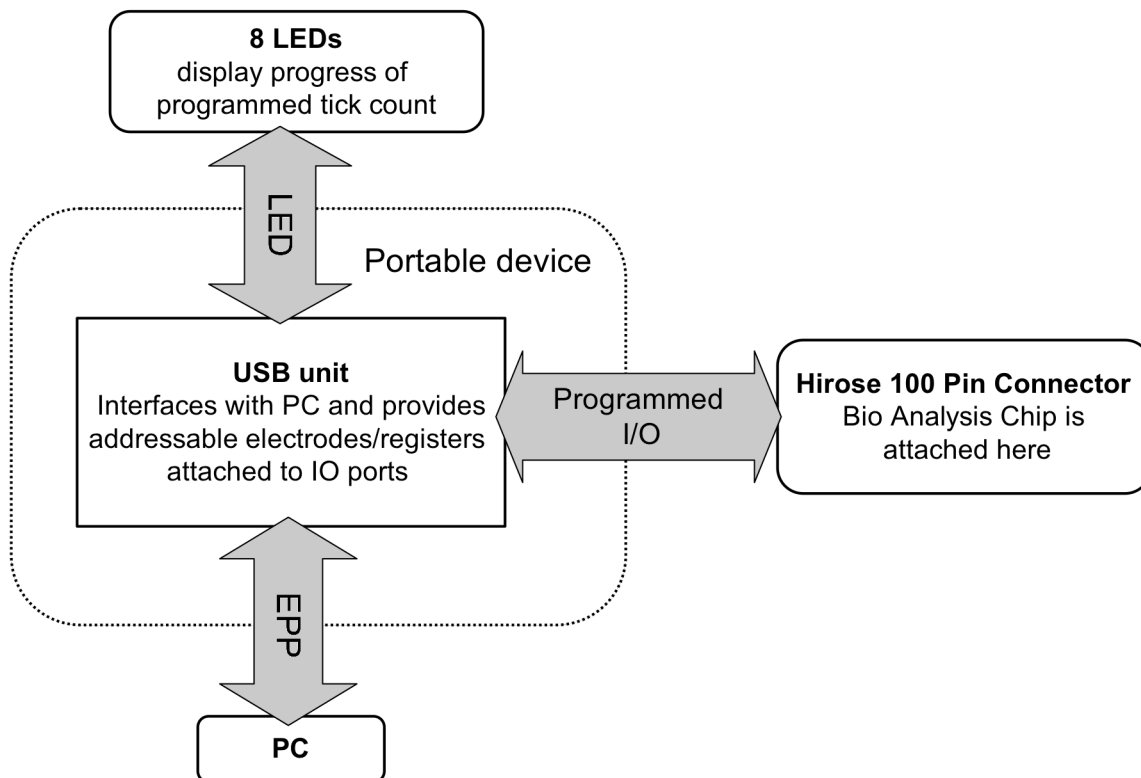


Figure 27. Top level block diagram of the FPGA based portable analysis device showing flow of information and electrical signalling.

## 8.2 Programming and Operation

For USB communication, Application Programming Interfaces (APIs) defined in Digilent's "dpcutil.dll" file are used. A Dynamic Link Library (DLL) file such as this contains code and data that can be used in developing software. These programming

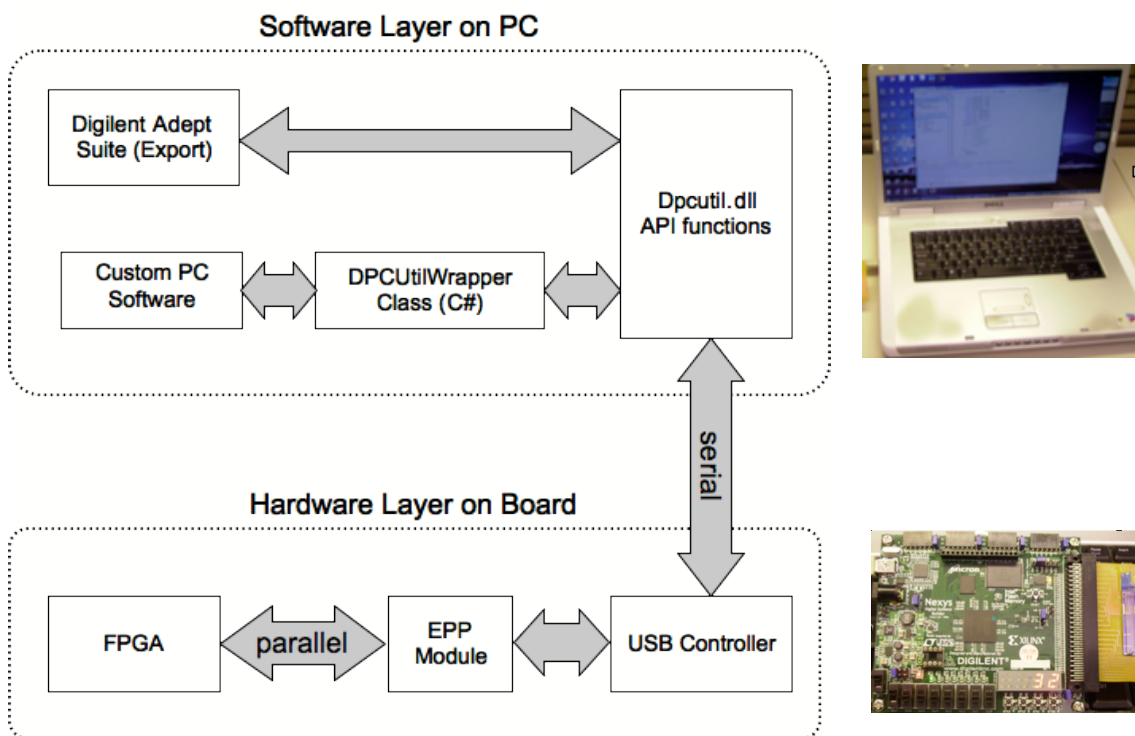


Figure 28. Software and hardware components of the portable device programming and their communication channels.

methods are present in the DPCUtilWrapper class (a programming language construct used to group related methods and fields). The Digilent Adept Suite is used for transferring the compiled Verilog program to the FPGA using ExPort (Fig. 28). The



dpcutil.dll being used by the custom software is a part of this suite. The software application developed in-house (Fig. 29) using the C# programming language calls certain methods of dpcutil.dll to communicate with the USB port of the computer. Data is sent through the USB cable to the connected FPGA board. The library file (dpcutil.dll) marshalls the data for sending over the USB cable. The onboard Cypress USB controller handles the USB communication and offers the user an enhanced parallel interface to the FPGA, thus essentially de-marshalling the data for the FPGA.

The `UsbComm` class contains methods to initialize the device. To initialize communication `DPCInit()` API is called, and if successful the `DPCGetDevBName()`, and `DPCGetDevType()` APIs are invoked to get information on the devices on the board. Once the user selects the recognized device, `DpcOpenData()` is used to open the communications channel. To stop the device communications, `DpcCloseData()` is called and `DpcTerm()` is called to close the connection with the device. These steps are done using the graphical user interface generated in C# (Fig. 29). The step-by-step procedure for operating the device is outlined in the Use Case diagram in Fig. 30.

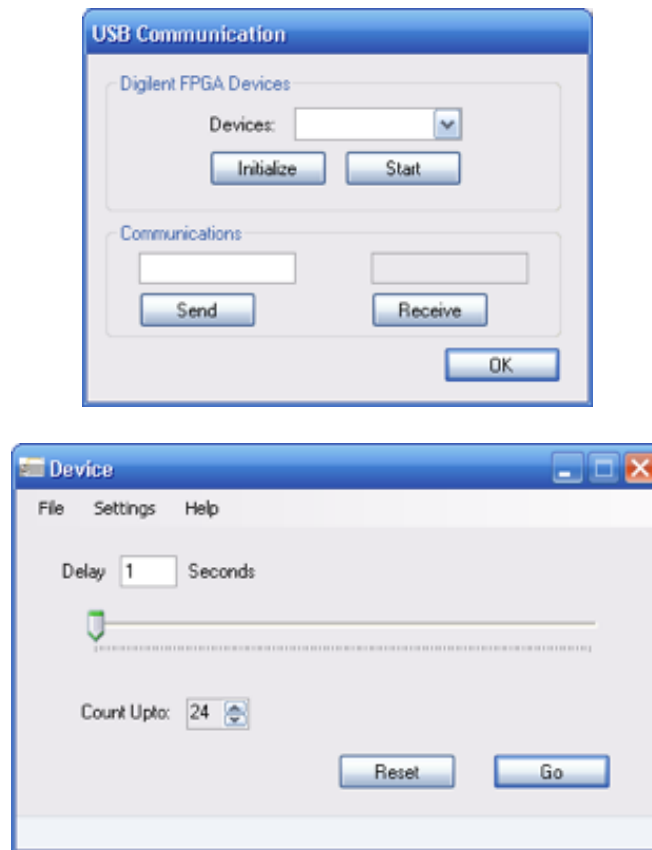
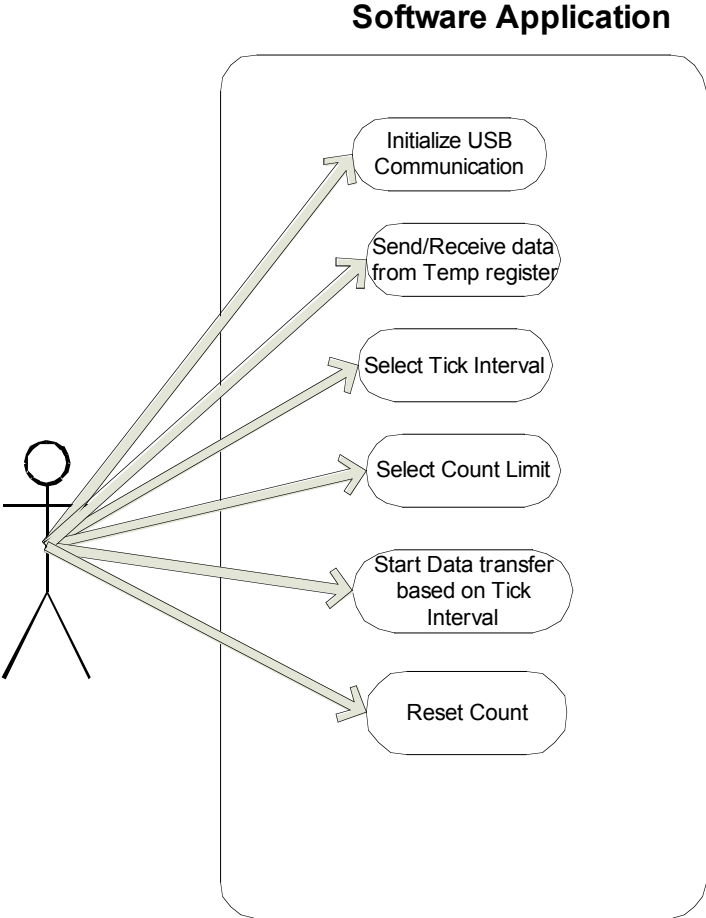


Figure 29. Screenshots of USB communication initialization window and the capture-release window showing the user input for the time of each capture and the number of capture-release steps to be taken.



Use case	Details
Initialize USB communication	The user selects “USB Communication...” in the menu of the application and initializes the USB communication with the desired FPGA device. The USB Communications need to be initialized for all of the subsequent use cases
Send Receive Data from Temp register	The User can specify data to be written to the temp register on the FPGA. The user enters the value in the textbox above the Send Button to send data to the Temp Register. Once the Receive button is pressed the data in the register is read back into the textbox above it.
Select Tick Interval	The user selects the Tick Interval or the Delay by either entering the value in the Delay textbox or by dragging the slider below it across. Note the delay is measured in seconds. The default value is 1 second. This value is the interval after which the next set of data is sent to the device

Figure 30. The Use Case diagram with details of each step.

Use case	Details
Select Count Limit	The user selects the Count Limit by entering the value in the “Count upto” scroll box. The upper limit for this is 24 .
Start Data transfer based on Tick Interval	The user presses the “Go” button on the application. The application starts the counter based on the requested parameters and send the appropriate mask to the FPGA registers which get pushed to the bioanalysis device
Reset Count	The user presses the “Reset” button. This clears all the counters and reinitializes the device.

Figure 30 Continued.

The programmable interface provides flexibility in incorporating additional components to the handheld device. Incorporation of LEDs, photodetectors and microfluidic pumps requiring electrical input can be envisioned to be integrated into the handheld device imparting additional functionality and versatility. An optimized and integrated device would eventually lead to a completely integrated portable bioanalysis device.

## CHAPTER IX

### CONCLUSIONS

Issues associated with analysis and detection of minute sample quantities continue to pose challenges in the development of advanced miniaturized biosensors and bioassays. The technique presented here is broadly applicable and provides a highly efficient and robust mechanism for “digitally” collecting and metering precise quantities of charged biomolecules (DNA, proteins, peptides, etc.) in a low-power format suitable for use in battery operated lab-on-a-chip systems. The use of very low potentials and currents (for example, a single AA battery would deliver sufficient power to perform multiple concentration and metering operations) combined with a relatively simple design taking full advantage of the cost benefits of photolithographic fabrication make the electrode mediated focusing technique presented here ideally suited to meet these needs. The electrode array was used to effectively collect, concentrate, focus, purify, meter, and inject DNA into microchannels for analysis providing a multifunctional and robust sample processing technique for on-chip bioanalysis assays (Fig 31). If used and optimized for all these processes, it would result in the simplification of the design of microfluidic devices as multiple sample preparation and analytical operations could be carried out at a single on-chip location. This would reduce the complexity of integrated microfluidic sample-to-results-chip designs by reducing the individual components currently needed to carry out each of these functions.

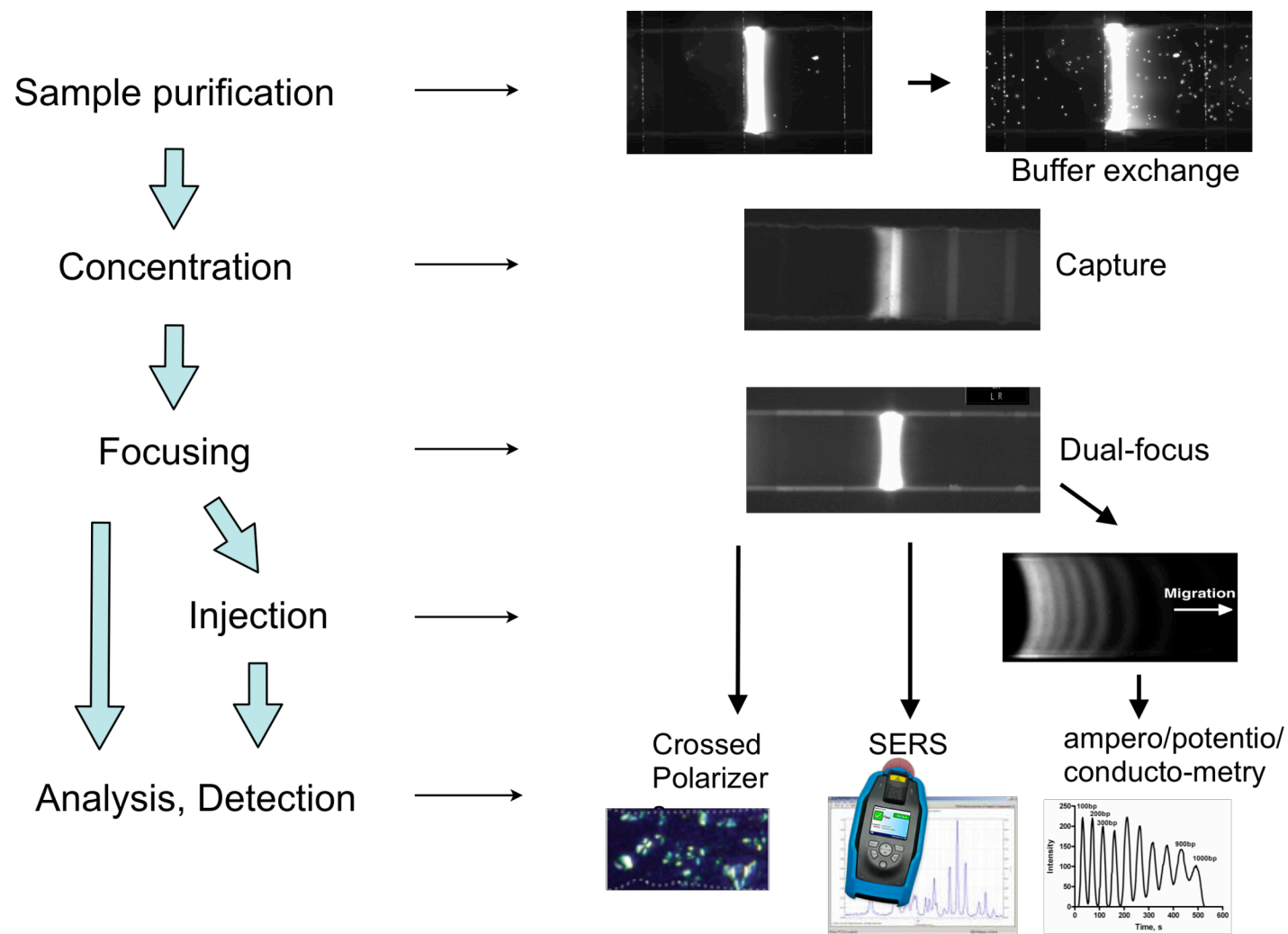


Figure 31. Applicability of the Capture-Release electrode array to multiple on-chip operations described in this work.

In addition to achieving the objectives of the research project, a new method to sensitively detect label-free charged biomolecules was developed that was based on scattering of light by the concentrated captured biomolecules at the capture electrode using any white light source. The analytes can essentially be detected in free solution as they can be captured or released into the solution by simply switching the applied voltage on or off. This method needs further investigation to optimize and characterize the process to make it amenable to a variety of interesting applications. Nevertheless, it promises to have implications in biodetection technologies of the future.

## REFERENCES

1. Luckey, J. A., Norris, T. B., & Smith, L. M. (1993) *Journal of Physical Chemistry* 97, 3067-3075.
2. Manz, A., Harrison, D. J., Verpoorte, E. M. J., Fettinger, J. C., Paulus, A., Ludi, H., & Widmer, H. M. (1992) *Journal of Chromatography* 593, 253-258.
3. Harrison, D. J., Fluri, K., Seiler, K., Fan, Z. H., Effenhauser, C. S., & Manz, A. (1993) *Science* 261, 895-897.
4. Harrison, D. J., Manz, A., Fan, Z. H., Ludi, H., & Widmer, H. M. (1992) *Analytical Chemistry* 64, 1926-1932.
5. Effenhauser, C. S., Manz, A., & Widmer, H. M. (1993) *Analytical Chemistry* 65, 2637-2642.
6. Jacobson, S. C., Hergenroder, R., Koutny, L. B., Warmack, R. J., & Ramsey, J. M. (1994) *Analytical Chemistry* 66, 1107-1113.
7. Khandurina, J., Jacobson, S. C., Waters, L. C., Foote, R. S., & Ramsey, J. M. (1999) *Analytical Chemistry* 71, 1815-1819.
8. Song, S., Singh, A. K., & Kirby, B. J. (2004) *Analytical Chemistry* 76, 4589-4592.
9. Lin, Y. C., Ho, H. C., Tseng, C. K., & Hou, S. Q. (2001) *Journal of Micromechanics and Microengineering* 11, 189-194.
10. Lapos, J. A. & Ewing, A. G. (2000) *Analytical Chemistry* 72, 4598-4602.



11. Roddy, E. S., Lapos, J. A., & Ewing, A. G. (2003) *Journal of Chromatography A* 1004, 217-224.
12. Zhang, C. X. & Manz, A. (2001) *Analytical Chemistry* 73, 2656-2662.
13. Jacobson, S. C. & Ramsey, J. M. (1995) *Electrophoresis* 16, 481-486.
14. Jung, B., Bharadwaj, R., & Santiago, J. G. (2003) *Electrophoresis* 24, 3476-3483.
15. Kim, D. K. & Kang, S. H. (2005) *Journal of Chromatography A* 1064, 121-127.
16. Kurnik, R. T., Boone, T. D., Nguyen, U., Ricco, A. J., & Williams, S. J. (2003) *Lab on a Chip* 3, 86-92.
17. Vazquez, M., McKinley, G., Mitnik, L., Desmarais, S., Matsudaira, P., & Ehrlich, D. (2002) *Journal of Chromatography B-Analytical Technologies in the Biomedical and Life Sciences* 779, 163-171.
18. Huang, X. J., Pu, Q. S., & Fang, Z. L. (2001) *Analyst* 126, 281-284.
19. Smith, E. M., Xu, H. W., & Ewing, A. G. (2001) *Electrophoresis* 22, 363-370.
20. Slentz, B. E., Penner, N. A., & Regnier, F. (2002) *Analytical Chemistry* 74, 4835-4840.
21. Lee, N. Y., Yamada, M., & Seki, M. (2004) *Analytical Sciences* 20, 483-487.
22. Backofen, U., Matysik, F. M., & Lunte, C. E. (2002) *Analytical Chemistry* 74, 4054-4059.
23. Asbury, C. L., Diercks, A. H., & van den Engh, G. (2002) *Electrophoresis* 23, 2658-2666.
24. Asbury, C. L. & van den Engh, G. (1998) *Biophysical Journal* 74, 1024-1030.

25. Chou, C.-F., Tegenfeldt, J. O., Bakajin, O., Chan, S. S., Cox, E. C., Darnton, N., Duke, T., & Austin, R. H. (2002) *Biophysical Journal* 83, 2170-2179.
26. Cannon, D. M., Kuo, T. C., Bohn, P. W., & Sweedler, J. V. (2003) *Analytical Chemistry* 75, 2224-2230.
27. Dai, J. H., Ito, T., Sun, L., & Crooks, R. M. (2003) *Journal of the American Chemical Society* 125, 13026-13027.
28. Wang, Y.-C., Stevens, A. L., & Han, J. (2005) *Analytical Chemistry* 77, 4293-4299.
29. Edman, C. F., Raymond, D. E., Wu, D. J., Tu, E., Sosnowski, R. G., Butler, W. F., Nerenberg, M., & Heller, M. J. (1997) *Nucleic Acids Research* 25, 4907-4914.
30. Heller, M. J. (2002) *Annu. Rev. Biomed. Eng.* 4, 129-153.
31. Heller, M. J., Forster, A. H., & Tu, E. (2000) *Electrophoresis* 21, 157-164.
32. Sosnowski, R. G., Tu, E., Butler, W. F., O'Connell, J. P., & Heller, M. J. (1997) *Proceedings of the National Academy of Sciences of the United States of America* 94, 1119-1123.
33. Brahmasandra, S. N., Ugaz, V. M., Burke, D. T., Mastrangelo, C. H., & Burns, M. A. (2001) *Electrophoresis* 22, 300-311.
34. Lin, R., Burke, D. T., & Burns, M. A. (2003) *Journal of Chromatography A* 1010, 255-268.
35. Lin, R., Burke, D. T., & Burns, M. A. (2005) *Analytical Chemistry* 77, 4338-4347.

36. Stellwagen, N. C., Gelfi, C., & Righetti, P. G. (1997) *Biopolymers* 42, 687-703.
37. McKnight, T. E., Culbertson, C. T., Jacobson, S. C., & Ramsey, J. M. (2001) *Analytical Chemistry* 73, 4045-4049.
38. Kirby, B. J. & Hasselbrink, E. F. (2004) *Electrophoresis* 25, 187-202.
39. Patankar, N. A. & Hu, H. H. (1998) *Analytical Chemistry* 70, 1878-1881.
40. Beckers, J. L. (2000) *Electrophoresis* 21, 2788-2796.
41. Brahmasandra, S. N., Burke, D. T., Mastrangelo, C. H., & Burns, M. A. (2001) *Electrophoresis* 22, 1046-1062.
42. Stellwagen, N. C., Gelfi, C., & Righetti, P. G. (1997) *Biopolymers* 42, 687-703.
43. Stellwagen, E. & Stellwagen, N. C. (2003) *Biophysical Journal* 84, 1855-1866.
44. Morgensen, K. B., Klank, H., & Kutter, J. P. (2004) *Electrophoresis* 25, 3498-3512.
45. Wang, J. (2005) *Electroanalysis* 17, 1133-1140.
46. Drummond, T. G., Hill, M. G., & Barton, J. K. (2003) *Nature Biotechnology* 21, 1192-1199.
47. Vandaveer IV, W. R., Pisas-Farmer, S. A., Fischer, D. J., Frankenfeld, C. N., & Lunte, S. M. (2004) *Electrophoresis* 25, 3528-3549.
48. Woolley, A. T., Lao, K. Q., Glazer, A. N., & Mathies, R. A. (1998) *Analytical Chemistry* 70, 684-688.
49. Lazar, I. M., Grym, J., & Foret, F. (2006) *Mass Spectrometry Reviews* 25, 573-594.

50. Shaikh, F. A. & Ugaz, V. M. (2006) *Proceedings of the National Academy of Sciences of the United States of America* 103, 4825-4830.
51. Livolant, F. & Leforestier, A. (1996) *Progress in Polymer Science* 21, 1115-1164.
52. Livolant, F. & Leforestier, A. (1996) *Progress in Polymer Science* 21, 1115-1164.
53. Rill, R. L., Strzelecka, T. E., Davidson, M. W., & Van Winkle, D. H. (1991) *Physica A* 176, 87-116.
54. Robinson, C. (1961) *Tetrahedron* 13, 219-234.
55. Leforestier, A. & Livolant, F. (1993) *Biophysical Journal* 65, 56-72.
56. Livolant, F. (1991) *Physica A* 176, 117-137.
57. Reich, Z., Wachtel, E. J., & Minsky, A. (1994) *Science* 264, 1460-1463.
58. Kassapidou, K., Heenan, R. K., Jesse, W., Kuil, M. E., & van der Maarel, J. R. C. (1995) *Macromolecules* 28, 3230-3239.
59. Kassapidou, K., Jesse, W., van Dijk, J. A. P. P., & van der Maarel, J. R. C. (1998) *Biopolymers* 46, 31-37.
60. Khokhlov, A. R. & Semenov, A. N. (1981) *Physica A* 108, 546-556.
61. Khokhlov, A. R. & Semenov, A. N. (1982) *Physica A* 112, 605-614.
62. Lo, R. C. & Ugaz, V. M. (2006) *Electrophoresis* 27, 373-386.
63. Durand, D., Doucet, J., & Livolant, F. (1992) *Journal de Physique II (France)* 2, 1769-1783.

## APPENDIX A

## PRINTED CIRCUIT BOARD FABRICATION PROCEDURE

To generate the electrical interface between the voltage source power supply and the silicon-glass microfluidic device, we use a ribbon cable attachment and fabricate a Printed Circuit Board (PCB). To transfer the circuit design to the PCB, the circuit is first printed onto a transparency using a laser or inkjet printer and this pattern is then transferred to the presensitized PCB (Injectorall Electronics Corp., Bohemia, NY) using the following procedure:

The following two solutions are required for the procedure:

1. Developer solution: 500 ml DI water + 3-3.5 ml NaOH solution
2. Ammonium Peroxydisulfate solution: 150 gm Ammonium Peroxydisulfate (Fisher Scientific, NJ) per liter of solution. Add the crystals to DI water and heat at a low setting and stir continuously. Make sure no fumes are coming out.

The stepwise procedure for patterning the PCB is as follows:

1. Take Ammonium Peroxydisulfate solution in a 1000 ml flask and heat it on lowest setting on the heating plate in the fume hood with stirring for 15-20 minutes before using it.
2. Three devices of the circuit designs generally fit in it, so cut the PCB accordingly.
3. Start the UV light and wait for it to warm up a little. Peel off the protective film on the PCB (preferably in a dark room) to expose the UV-sensitive coating and place the transparency with the printed circuit design, on top of it followed by a thick glass

plate, to secure the transparency to the pc-board. Make-sure the transparency is not showing the mirror-image of the desired design.

4. Expose the setup to UV light for 1.5 mins.
5. Take the pc-board and dip it in the developer solution in a glass dish and rock the glass dish for a couple of minutes till the exposed pattern appears and all exposed photoresist coating comes off.
6. Rinse with DI water, and dip it in the heated Ammonium Persulfate solution in the fume hood (this solution should be continuously heated and stirred at the slowest setting).
7. After ~15 minutes inspect the PCB's to check the pattern/etch.
8. Rinse off the polymerized pattern with acetone to reveal the copper pattern.

APPENDIX B  
FABRICATION OF SILICON DEVICES

The procedure for silicon wafer processing employed is as follows:

1. Mask Aligner : Prior to turning on the mask aligner, make sure the large chuck and plate are installed. (Make sure the air is off prior to doing this, then turn the air back on after they are installed. You will have to turn the air off/on outside of the cleanroom.) When placing the large plate onto the aligner, you will need to place the blue folded wipes underneath each of the 4 corners and replace only one screw into each corner. If this is not done, the chuck+wafer will not fit underneath the plate. Turn on the aligner and light source (black box = the light source needs to reach 375 light intensity units prior to use.) Make sure the vacuum is working. (push the chuck into place in the aligner – you will be able to hear the vacuum if it is operating.
2. Clean Wafer: Clean a 6 inch silicon wafer (shiny side) either with IPA and acetone or by using the Reactive Ion Etcher (RIE). The parameters for RIE are: 70% gas 2 (O<sub>2</sub>); Pwr = 100W; Time = 5 minutes; Base Pressure = 80
3. HMDS: Place aluminum foil in spin coater 'bowl.' Place the wafer in the spin coater and cover with the Microposit HMDS. Make sure vacuum is on. Spin at 3000 rpm for 60 seconds.
4. Photoresist: Cover the wafer with Shipley 1827 photoresist (positive resist = Photoresist in which photoresist molecules in the resist become soluble in areas exposed to ultraviolet light. These molecules are washed away in the developer

solution during the development step). You will need 2-3 plastic bulb pipets full. Spin at 3000 rpm for 30 seconds.

5. Softbake: Place the wafer on a hotplate at 100C for 5 minutes.
6. Exposure: Set exposure time by pressing the <enter> key, then <main menu> key, <exp time>, <ins>. Then enter the desired time (units are seconds.) Pull the chuck out and place the wafer on the aligner chuck. Push in the chuck. Place the mask on the aligner, chrome side down. Press <Mask Vacuum> on. Press <Load>. Pull the light over the mask. Press <Head Lock>. Press <Contact>, Press <Expose>.
7. Development: Use MF-319. Pour some developer in a glass dish. Put the wafer in the dish and swirl carefully for ~1.5-3 minutes. Rinse with Millipore water, 1.5-3 min. Air dry wafer.
8. Descum: RIE with the same settings as for cleaning step, except with the time being set at 10 seconds. This step essentially removes any remnant of the photoresist in the exposed pattern if it remains after the development step.
9. Hardbake: Put on a hotplate at 100C for 1-2 minutes. Let cool then place in a wafer holder.
10. Metal Deposition: Deposit either 500A titanium (bottom) /1000A platinum or 500A chrome (bottom) /1000A gold. The chrome/gold deposition can be done in house. For Ti/Pt deposition, the wafers need to be placed in wafer holders, wrapped in bubble wrap and sent to Lance Goddard Associates (Foster City, CA)



11. Liftoff: Place wafer in a glass dish with some acetone covering the wafer. Swirl/let sit for at least 5 minutes. After metal starts lifting, take a swab and rub off excess metal. Rinse with Millipore water 1.5-3 minutes, Dry with air.

Notes by René D.Elms and :

1. Exposure time: An exposure time of 60s seems to be ideal with the spin coating parameters employed.. Trials with 30s resulted in underexposed patterns – the pattern was lost during developing. Trials with 90s resulted in overexposed patterns – after metal deposition, no metal would liftoff.

2. Metal Deposition: Problems have been encountered with platinum (Pt) deposition. The first batches sent to Lance Goddard for Pt deposition (via sputtering) had an uneven Pt surface with bubbles and a crackled appearance. It was difficult to impossible to liftoff the metal, even with sonication and a Pt etchant. With the next batch, Pt was deposited using evaporation, but during use, the metal quickly degrades and comes off of the devices.

3. When depositing Pt via sputtering, it is so hot that it cooks the photoresist. (Heat from the source for evaporation also gets hot, but for sputtering. A possible/suggested solution is to use a thicker resist layer. Also, sputtering coats the side walls (around edge of the wafer) and that makes it hard for the solvent to get under the photoresist for lift-off. Evaporation is better for the sidewall coverage (3x6inch wafers/run.) But, there is a lower kinetic energy, so the metal tends not to stick as well. Adhesion is much better for sputtering.

4. The descum step may not be necessary for our purposes. In case the deposition doesn't turn out well, try the procedure without the de-scum step and make sure the initial wafer cleaning and UV exposure values are in order.

## APPENDIX C

### MASK ALIGNER INSTRUCTIONS

In the Materials Characterization Facility's clean room, Mask aligner Q-4000, made by Quintel Company is available for UV lithography. For UV light source this instrument employ 350 WATT Hg Short ARC lamp (Advanced Radiation Corporation), which provide most intensive UV light peak from 360 to 400 nm of wavelength. Q-4000 system provides  $\sim 400 \text{ cm}^2$  of evenly distributed UV light field. With normal setting of the instrument a UV light intensity reading with UV light meter is about  $12 \text{ mW/cm}^2$

Step-by-step operation procedure for mask aligner Q-4000:

1. Turn Power On from UV light power supply (UVPS).
2. After 3-4 minutes ignite the lamp and then hold start button on UVPS for about 2-3 seconds. The arrows on both scales should rise up.
3. Let the UVPS warm up for about 15-30 minutes.
4. Press POWER on Mask Aligner.
5. Press ENTER on dialog panel that located on the right side of the power switch, to get access to MAIN MENU.
6. Press 1 to get access to EXPOSURE TIME\* options. For loading desirable exposure time press INS (0) button, then appropriate numbers, and then ENTER.
7. Put mask on face of mask aligner.

8. Press MASK VACUUM button. Make sure that the mask is sticking due to vacuum, onto the mask holder.
9. Pull out sample tray and place your wafer\*\* onto the chuck, then press LOAD button (chuck vacuum should start working). To stop vacuum press CLEAR button.
10. Push tray in when you are ready.
11. Wait until serial of message in dialog window will finish with message SEPARATION, then press SEPARATE button on the left side of the tray. If you need to align your substrate under mask, use joystick on the right side. For the optical inspection use joystick on the left side of the chuck.
12. Wait until message CONTACT appears in dialog window, then rotate optical head into position over your mask, press HEAD LOCK button (below POWER button), then press EXPOSE button (located below dialog window).
13. Wait until your exposure process finishes (avoid any eye contact with UV light) UNLOAD WAFER message should appear in dialog window, then press HEAD LOCK again, rotate optical head back, and pull out a tray with your sample.
14. Switch off UV light power supply.
15. Press ENTER in dialog window, then press 6 (power off) to shut down the instrument.

\* For your references and exposure time calculation you need to know actual intensity under mask aligner lens during exposure. For this, use Radiometer VLX

365 UV light intensity meter. Place sensor directly into UV light field\*\*\*. Switch on the meter box. You will see intensity reading in milliWatts per square centimeter. This intensity value is at a wave length of 365 nm. The exposure energy ( $\text{mJ}/\text{cm}^2$ ) is equal intensity ( $\text{mW}/\text{cm}^2$ ), that is multiplied by exposure times in seconds:  
 $\text{mJ}/\text{cm}^2 = \text{mW}/\text{cm}^2 \times \text{sec}$ .

\*\* Maximum thickness of substrate that can be accommodated on a standard configuration machine is 6.3mm or 0.25 inch

\*\*\* To have access to the UV light exposure field with unlimited amount of time you need to get in manual mode. From main menu choose #4 CONTROLS. From *Controls* menu choose EXPOSURE TEST ON and press 3. Wait for lens unit to lift up. Then press 2 (MANUAL SHUTTER ON). Place UV light meter sensor under the lens. When you finish the measurement, take out sensor, press 2 (MANUAL SHUTTER OFF), and then 3 (EXPOSURE TEST OFF) and press ENTER to exit the controls menu.

## APPENDIX D

### FABRICATION OF GLASS CHANNELS

The glass wafer etching procedure to fabricate the glass channels used in this work is described here. All procedures were conducted in the Materials Characterization Facility (Room 304, JEB Engineering Building) at Texas A&M University unless otherwise noted.

#### Materials:

- 6 inch Borofloat wafers
- Chrome (Cr) etch: Cr-14S
- Gold (Au) etchant
- Full strength hydrogen fluoride (HF): When fresh HF is used, the etch rate is ~5-7  $\mu\text{m}/\text{min}$ .
- water,
- Shipley 1827
- HMDS
- MF-319 developer
- Acetone

NOTE: Use Trionic gloves, apron, and face shield when using the etchants. These chemicals are extremely caustic and must be used under the hood.

Procedure:

1. Anneal Borofloat Wafers: Place wafer(s) in oven at ~650 degrees Celsius for 30-60 minutes. Label each wafer (use a scribe) so it can be followed through the process.
2. Clean wafers in the RIE (same program as for Silicon wafers.) Pack it for shipping.
3. Metal Deposition on Wafers: Deposit 600 Angstroms Chrome (bottom layer) and 4000 Angstroms Gold onto the annealed wafers by thermal evaporation (this can be done at Lance Goddard and Associates).
4. Patterning: The photoresist used is Shipley 1827 (a positive resist.) The patterning procedure is the same as for silicon wafer patterning, except there is an extra hardbake at 110 C for 30 minutes after the pattern is developed.
5. Height of pattern: Once the wafer is cooled, use the profilometer to check the height of the patterned photoresist. You will need this for step 9 in order to know how much true depth has been etched.
6. Setup: Set up 4 containers in the hood (8x8x8 inches polypropylene square containers in MCF) and fill them with: 1.) Au etch, 2.) Cr etch, 3.) HF, 4.) Water rinse

7. Gold Etch: Using a container, place the wafer in the Au etch for ~3- 7 minutes. You will be able to see the chrome underneath if it has etched enough. Then place the wafer in the water rinse for ~ 3 minutes.
8. Chrome Etch: Using a container, place the wafer in the Cr etch for ~5-12 minutes. You will be able to see through to the glass if this is done correctly. Then place the wafer in the rinse for 3 minutes. While the wafer is in the HF etching the glass, dump the water rinse container and refill with fresh water.
9. Glass Etch: Use HF in a polypropylene container. The first wafer in the batch must be processed much more slowly. Since the etch rate of HF changes with time, you must first etch in HF for a shorter period (5 minutes). Then place the wafer in the water rinse for 5 minutes. Dry the wafer and check with the profilometer for the etch depth. Calculate the etch rate and how much longer is needed to achieve the desired depth. (50  $\mu\text{m}$  for typical channels). Place the wafer back in the HF for the appropriate time calculated above. Water rinse for 5 minutes, then dry it and check etched depth with profilometer. If the depth is still not enough, recalculate, and continue the same process until desired depth is achieved. After you reach the desired depth, use all the accumulated HF times for the glass etch/HF etch time for the rest of the batch.
10. Strip photoresist using acetone.
11. Strip Au: Place the wafer in the Au etchant for 3 minutes or until all the gold is stripped. Water rinse for 3 minutes



12. Dice using the dicing saw, then place the individual channels in a small beaker of Cr etchant (under a hood) until the Cr is removed. Rinse in water for 3-5 minutes.

## APPENDIX E

### WIRE BONDING PROCEDURE

A manual wire bonder (wedge bonder) from Kulicke & Soffa model 4523 was used to wire bond the PCB to the silicon devices on the microfabricated chip. The procedure to wire bond is as follows:

1. Power on both the bonding machine and an additional light source if available (the wire bonder has its own light source that may not be bright enough).
2. Load the preset program for bonding.
3. The clamp opens after Step 1 and closes at Step 2.
4. Click and hold the left key of the mouse. Move the tip to the first bonding site, press “Search” to get the tip close to the surface of the bonding site, and then release the key to connect the wire to the first bonding site.
5. Click and hold the left key again. Move the tip to the second bonding site and then release it to bond the wire to the second site.
6. Use high “loop” values (i.e., a larger loop made of a longer wire) to avoid circuit shortage since there may be some metal residue on the site of the silicon device from imperfect dicing (Appendix E).
7. A reference set of parameters that work well for wire bonding (1<sup>st</sup> bond is on the PCB, 2<sup>nd</sup> bond is on the gold electrodes on the silicon device) is given in the following table:

Table 3. The values of wire bonding parameters that were found to work well for the bonding of PCB and gold electrodes on silicon devices.

SCREEN 1	SCREEN2	SCREEN 3	SCREEN 4
SEARCH = 4.30	STEP = 4.3	SEARCH= 4.15	STANDARD
POWER=2.27	KINK = 0.0	POWER= 2.42	LONG
TIME=1.2	REVERSE = 0.0	TIME=2.0	LONG
FORCE= 1.1	Y-SPEED = 0.0	FORCE=1.7	ON
	LOOP = 7.0	TAIL = 9.9	
		TEAR=5.0	

Notes:

1. If the wire bond does not seem to stick to metal electrode, try increasing one or more of power, force and time. If the bond seems to break off, it implies that the wire bonding conditions are too harsh. Reduce the value of one or more of power, force and time.
2. Before clicking the mouse on the wire-bonder to make any bond, make sure that the tail/tip of the wire is extending right below the tip of the bonding needle and pointing towards you. This ensures that the wire gets ‘stamped’ correctly when you click the mouse to make the bond.
3. If the wire comes out of the bonding needle, the threading of the hole can be challenging considering it is microscopic. An easy way to do the threading would be to loosen the needle/wedge and rotate it 180 degrees along the vertical axis to reveal the threading hole located at the bottom (threading of the upper hole is relatively easy). Now once the hole is visible through the microscope, the threading can be done with lesser effort.

## APPENDIX F

## WAFER DICING OF SILICON AND GLASS WAFERS

The instructions for operating the Disco DAD-2H/T Dicing Saw to dice the silicon and glass wafers are as follows:

Warning: The dicing saw operates at very high spindle speeds (30,000 rpm) and at that speed the blade will cut quite quickly and deeply. In addition there is the possibility that the blade will fracture and impart fragments into your tissue. Please be very careful about keeping your fingers and samples away from the spinning spindle. Also it is quite difficult to determine if the spindle is spinning or not\*, so unless you know it has stopped, assume the spindle may be in motion. Wear safety glasses for your protection during operation process. If there is some problem at any time during operation of the dicing saw, press the EM STOP button to stop all motion of the saw.\*\*

The following is a general scheme for cutting silicon wafers and glass slides or wafers. If you need to cut something different or if you feel the blade needs to be changed please contact the person in charge of the equipment.

1. Sign in the log book for the dicing saw. Check status of instrument and blade.
2. Turn on water to the unit (blue handle currently located behind the unit) and make sure the tubing is reaching the sink.

3. Turn on compressed air to the unit (currently located as a hanging lever from the ceiling). You will hear compressed air flowing around the spindle bearings.
4. Turn on the power transformer located on the floor to the right of the unit. The power switch is on the back of the transformer.
5. Check the blade condition over the flange to check for blade damage.
6. If less than 1mm of blade is visible outside the flange edge, replace the blade\*\*\*.
7. Turn on the power breaker on the right hand side of the unit. The switch is directed 'up' when in the ON position.
8. The unit will power up and show EEE.. in the display. Press the C button to clear the display. At this point the CUT-STRK led should be flashing.
9. Enter the CUT-STRK type by entering a 1 or a 0. 0 indicates a square cutting pattern and 1 indicates a rounded cutting pattern.
10. After the pattern type enter the length of the cut stroke (in inches if the inches led is lit). Then press the W key to enter in the CUT-STRK. Once you press W the CUT-STRK led should stop flashing, if not you have entered an incorrect value for the CUT-STRK. Note: The CUT-STRK length should be  $\frac{1}{2}$  inch (~1 cm) longer than your sample size. If you are going to cut a 4 inch wafer use 4.5 inches. For a rectangular sample use  $\frac{1}{2}$  inch longer than the longer of the two axes.
11. Then the CUT-SPD led will be flashing and the box labeled BLOCK will indicate 1. (Block 1 and Block 2 refer to the two axes of cutting, for most entries

you will need to enter a value for both Block 1 and Block 2). The cut speed is entered by entering a predetermined number that is associated with a particular cutting speed. For standard silicon wafers CUT-SPD 12 was found to be a good value (cut speed 12 equals 7 mm/sec or 0.276 inch/sec) For glass slides cut speed 3 (1mm/sec or 0.04 inch/sec) is a good number. The full range of cut speeds is from 0 (0.3 mm/sec) to 58 (300 mm/sec) Please see the manual for the chart of the cutting speed values. After entering the CUT-SPD value, press W to write the entry into memory.

12. Now enter CUT-SPD for BLOCK 2 and press W when finished. Note: the cut speed is usually the same for both BLOCK1 and BLOCK2 but you may enter different values if appropriate. The Y-IND led should now be flashing.
13. The Y-IND value refers to the distance between cuts (again in inches or mm depending if the inches or mm led is lit). Enter the BLOCK1 value and press W.
14. Enter the BLOCK2 Y-IND value and press W. If you enter the same value for BLOCK1 and BLOCK2 Y-IND values you will cut each axes equally making squares.
15. Now the Z-IND BLOCK1 led should be flashing. The Z-IND refers to the height above the surface of the chuck you wish to cut. If the sample is mounted on the blue dicing tape (discussed below) and you wish to cut through the wafer, enter a number just smaller than the thickness of the tape. The tape in the MCF is 0.0035 inches thick, so entering a Z-IND BLOCK1 value of 0.003 (0.075mm) will cut through the wafer and 0.0005 into the surface of the tape. Press W to

enter the value. To partially score a sample determine the sample thickness and add the tape thickness to get a total thickness. The total thickness minus the depth you wish to score will equal the number you should enter for Z-IND

16. Enter the Z-IND BLOCK2 and press W. The Z-IND will usually be the same for BLOCK1 and BLOCK2.
17. Now Z-IND BLOCK7 will be flashing. BLOCK7 refers to the height above the chuck where the blade will not interfere with the sample. This number should be greater than the sum of the tape plus the sample. 0.27 (inches is a safe number for all samples thinner than  $\frac{1}{4}$  of an inch (10mm). Press W to enter the value.
18. Now Z-IND BLOCK8 will be flashing. This value is a parameter to account for blade wear during cutting. This is not a problem at the low volume we are cutting so enter 0.0002 (0.005mm) and press W.
19. The  $\Theta$ -IND should now be flashing. The  $\Theta$ -IND refers to the angle (in degrees) between BLOCK1 and BLOCK2. For most samples the  $\Theta$ -IND will be 90 degrees. Enter 90 and then press W.
20. Now CUT-NO BLOCK3 will be flashing. This number is tied to Z-IND BLOCK7 (blade wear parameter), to effectively turn off this feature enter 9999 and press W. This will mean after 9999 cuts the blade will move down 0.0002 inches to account for the wear in the blade. If you are cutting especially hard materials and want to use the blade wear parameters correctly consult MCF staff of the manual.

21. Now none of the led's should be flashing. To check the parameters you have just entered press SHIFT to scroll through the values. To change a value, press C/E re-enter the value and press W. Once you are satisfied with the parameters you can go to the SETUP routine. Note: The CUT-SPD values displayed will now show the inches/sec value instead of the cut code you originally entered.
22. To properly determine the blade diameter, the dicing saw slowly moves the blade towards the chuck until electrical contact is made. For this setup to occur, the chuck needs to be clean and dry with no sample mounted on it. Also press SPINDLE to start the spindle and press VACUUM (their led's should be lit). Then press SET UP and the system will automatically determine the blade diameter.
23. When the SET UP routine is finished. Press the INDEX button (5th from left on angled panel) Then press the Y← button (this moves the Y axis one Y-IND amount. Continue to press the Y← button until the blade and the objectives are moved to the back.
24. Now mount your sample, use one of the tape frames and apply blue tape so that it is tightly stretched across the frame. This will take practice and will require several tightening steps at different angles until the tape forms a flat plane across the frame.
25. Use a razor to trim the blue tape from the edges of the tape frame.
26. Place your sample in the middle of the tape frame so that it adheres to the adhesive. Turn the frame over to make sure the sample is firmly mounted to the



tape. Start from one edge of the sample and press the tape firmly onto the sample, trying to minimize air bubbles trapped underneath the sample. If there are some small air bubbles trapped under the sample. If you do not firmly affix the sample to the tape the diced pieces will be removed by the cooling water and you will lose them.

27. Press the VACUUM button to turn off the vacuum. Place the sample-loaded frame onto the chuck and center the sample as much as you can. Turn the VACUUM button back on to hold down the sample. With the sample on the chuck and the vacuum on, the vacuum gage should be in the green area. If not try to remount your sample.
28. Turn on the ILLUMINATION, the video monitor, and the line generator to be able to use the microscope to align your sample.
29. Press  $Y \rightarrow$  to move the blade and microscope objectives forward (one Y-IND at a time) until close to the edge or a cutting line of the sample. You can use the  $X \leftarrow$  and  $X \rightarrow$  to move the sliding table to position your sample under the objective. Once the edge of your sample is close to the objective light, press the JOG/SCAN button (6th from the left on tilted panel). Then using the  $Y \leftarrow$  and  $Y \rightarrow$  buttons you can move the sample back and forth small amounts.
30. Once you have found the edge (or cutting line) you will need to align the rotation of the sample using the JOG/SCAN (furthest button on right) and the  $\theta \cup$  and  $\theta \cap$  buttons to rotate the sample. By using a sample cutting line or edge and the  $\theta \cup$  and  $\theta \cap$  buttons; you can align the two in the split image video screen.

31. To test the alignment of the rotational direction use the X← and X→ keys to make sure the cut line/sample edge remains at the same horizontal position.
32. The blade will cut in between the two lines of the generator. Using the INDEX button and the Y← or Y→ direction make sure that your Y-IND spacing is correct (every time you move one Y-IND you should be directly on the next cut line).
33. Now use the Y-axis INDEX button and the Y← or Y→ keys to move to where you would like to place the first cut.
34. Press SEMI-AUTO (water from flange holder should come out over the blade)\*\*\*\*and the Y← (if your wafer is laying between you and blade) or Y→ (i operation will continue to make cuts spaced Y-IND BLOCK1 apart until you tell the unit to stop. Press SEMI-AUTO again to stop the cutting (the saw will continue to finish the current cut and then stop).
35. To cut in the BLOCK2 direction. Press the ROTATION button and then  $\theta \cup$  or  $\theta \cup$  to rotate the chuck to the BLOCK2 direction.
36. Press INDEX and Y← to move the stage back.

Shutting down the instrument: When you are finished using the dicing saw please

1. turn off the SPINDLE, ILLUMINATION,
2. turn off the video monitor and line generator
3. turn off the circuit breaker on the right side of the instrument,
4. turn off the transformer,
5. turn off compressed air

6. turn off the cooling water valve.

Please make sure the chuck is clean and dry (using the compressed air gun [this will need to be done before shutting off the compressed air] and/or paper towels).

\* Each flange set has holes in them for the wrench, so watch them to determine if spindle is rotating. If spindle is off, holes are visible, if not, flange ring looks gray without holes.

\*\* If the EM STOP button is pressed, you need to restart the dicing machine again. Switch off the power breaker on the right hand side of the unit, wait for 1 minute, then switch it back on and go through inputting all the settings again.

\*\*\*\* If water is not coming out to lubricate the blade, press SEMI-AUTO button again to stop the process and investigate if the water valve is open or closed.

## VITA

Name: Faisal Shaikh

Address: Artie McFerrin Department of Chemical Engineering, Texas A&M  
University, 3122 TAMU, College Station, TX 77843, USA

Email Address: dr.shaikh@gmail.com

Education: Ph.D., Chemical Engineering, Texas A&M University, College  
Station, Texas-77843, USA, 2008

B.En., Chemical Engineering, University of Mumbai, Institute of  
Chemical Technology (formerly U.D.C.T.), Mumbai, India, 2002